MULTIPHOTON GRIN ENDOSCOPY FOR REAL-TIME DIAGNOSIS OF DISEASED TISSUE

A Dissertation

Presented to the Faculty of the Graduate School

of Cornell University

In Partial Fulfillment of the Requirements for the Degree of

Doctor of Philosophy

by

David Maxim Huland

August 2014

MULTIPHOTON GRIN ENDOSCOPY FOR REAL-TIME DIAGNOSIS OF DISEASED TISSUE

David Maxim Huland, Ph. D.

Cornell University 2014

Multiphoton microscopy has the potential to become a valuable tool for clinical diagnosis of tissue health. It has the ability to provide images with similar cellular and architectural tissue information to the gold standard for tissue diagnosis, histopathological analysis of biopsies. However, unlike histopathology, it can provide these images in real time in unstained and unprocessed tissue *in vivo*. Due to the depth limitations of multiphoton microscopy, endoscopic access to the tissue is required for this technology to be clinically useful. This dissertation details our efforts to translate multiphoton microscopy into the clinical field through the development of a GRIN lens based multiphoton endoscopic prototype.

As compared to other endoscopic approaches, GRIN lenses, while rigid, provide several advantages, including small diameters (down to 0.350 mm), no need to miniaturize excitation and collection optics, low manufacturing costs and potential compatibility with existing biopsy instrumentation.

In this dissertation we initially show that multiphoton imaging through long (up to 285 mm) GRIN lens endoscope systems is possible. We then design fabricate a portable, rigid endoscope system suitable for imaging unstained tissues, potentially deep within the body, using a GRIN lens system of 1 mm diameter and 8 cm length.

The portable device is capable of imaging a ~200 μm diameter field of view at 4 frames/s. The lateral and axial resolution in water is 0.85 μm and 7.4 μm respectively.

We demonstrate the capabilities of our device through *in vivo* imaging of unstained tissues in live, anesthetized rats. We further show compatibility of this device with three photon excitation. Finally, we test the diagnostic capabilities of our prototype on human prostate cancer samples *ex vivo*. The presented results show great promise for GRIN endoscopy to become a valuable tool clinically both for the diagnosis of tissue health and to aid during surgeries by identifying tumor margins and other tissue architecture.

BIOGRAPHICAL SKETCH

David Maxim Huland was born in Hamburg, Germany and raised in Hamburg and Berlin, Germany. David is the son of Edith and Hartwig Huland, and the older brother of Chris Birgin Huland. With both his parents being medical doctors working in an academic setting, he was always fascinated by the advances in biomedical research and the possibilities and opportunities that advances in technology can offer to the medical field.

In the Fall of 2002, David enrolled at Cornell University and taking a heavy course load graduated with a dual degree, B.S. in Biological Engineering and B.S. in Biology in 2006. Wanting more training on medical devices, he enrolled in the M. Eng. program in Biomedical Engineering at Cornell University and completed a design project under Prof. Chris Schaffer in August 2007. After a year of working in Hamburg at his mother's pharmaceutical start-up, Immunservice GmbH, he decided to return to Ithaca, NY in August 2008 to pursue a Ph.D. in Prof. Chris Xu's research group, and has been working on GRIN multiphoton endoscopy ever since.

For Oma, Opa, Mom, Dad, Chris, Sisca and Luca

ACKNOWLEDGMENTS

I would like to thank numerous wonderful scientists, friends and family members for their support and mentorship that made this PhD possible. I am deeply grateful to my advisor, Prof. Chris Xu, for his continued support and advice. Learning from him, particularly from his exceptionally rational and efficient approach to problems, has made me grow significantly as a scientist and as a person over the last 6 years. The support he is able to provide to his graduate students, both financially and as a mentor, allows his students to focus on their research and professional development in an incomparable way. His career as a scientist is an inspiration to his group and a motivator to produce the best science possible. Additionally, I sincerely thank Prof. Chris Schaffer and Prof. Alexander Nikitin for their support and advice as members of my special committee.

I also want to thank all the members of the Xu and Webb research groups for their help and support in my research. Specifically, I thank Scott Howard, Mike Durst, David Rivera, Demirhan Kobat, Ji Cheng, Jen Lee and Adam Straub for introducing me to the lab and their immense help and patience as I learned how an optics laboratory functions. Thank you also to Kriti Charan, Nicholas Horton, Li-Chung Cheng, Ke Wang, Tianyu Wang, Tomas Rojo, David Sinefeld, Chris Brown and Ina Pavlova for their continued support, help and friendship throughout my PhD. Finally, thank you to Dimitre Ouzounov whose help and brilliance as a scientist and as a person has been invaluable to my studies.

I also want to thank the numerous excellent collaborators I've had the pleasure of working with over the years, amongst them Nozomi Nishimura, Jason Jones, Douglas Scherr, Ash Tewari, Sushmita Mukherjee, Ranjith Ramasamy, Wendy Williams and many more. It has been a tremendous pleasure to interact with all of you, both in our labs and offices, and outside of them too. Additionally, this PhD wouldn't have been possible, if it wasn't for the support network of my friends in Ithaca and abroad; and of course my girlfriend, Sisca, and our dog, Luca, who made the time outside of lab so much more meaningful and enjoyable. Finally, I want to thank my family. I am immensely grateful to have grown up in such a supportive and loving family and cannot thank you enough. Mom, Dad and Chris, you are the best family someone could wish for!

TABLE OF CONTENTS

LIST OF FIGURES

LIST OF TABLES

CHAPTER 1

INTRODUCTION

1.1 Cancer Diagnosis

Cancer is a major public health problem in the United States and abroad. Approximately one in 4 deaths in the United States is due to cancer with over 1.6 million new cases and over half a million deaths projected to occur in 2014 [1]. In the case of most cancers, early and accurate diagnosis can significantly improve the prognosis and help determine the most effective course of treatment. The first indication for a potential cancer diagnosis for most cancers comes from initial tests, such as a physical exam or a laboratory test for tumor markers. Low resolution imaging test such as an x-ray, a computerized tomography (CT), or a magnetic resonance image (MRI) can provide further information about the chance of cancer presence and the extent of the disease. However, while very effective at raising a general suspicion for cancer, these procedures generally cannot give a final diagnosis. The gold standard for ultimately providing a diagnosis is the tissue biopsy with histological processing and subsequent analysis by a trained pathologist under a white light microscope.

While very accurate and very well established, histopathology can take several days to weeks before a diagnosis is known. This is valuable time during which a therapy could have already been started and the patient suffers great discomfort waiting on their potential cancer diagnosis. Further, if this time could be reduced to

the order of minutes or less, histopathological findings could become a significantly stronger influence intra-operatively, providing valuable information to the surgeons that may aid them in margin assessment and other cellular structure identification.

This dissertation will detail our efforts to translate multiphoton microscopy (MPM) into the clinical field. MPM is a technology that has been predominantly used in academic research and can provide very similar cellular and architectural tissue information as the gold standard histopathology, but in real time and in unstained, unprocessed tissues *in vivo*. We will describe our instrumentation development up to the point of testing our prototype on *ex vivo* human samples of prostate cancer. While this technology is applicable to many different types of cancers, the focus of this dissertation will be on the example of prostate cancer for simplicity's sake. Many of the findings here, though, should translate to other cancers or diseases where a biopsy is a critical component of the diagnosis or where intra-operative margin assessment or tissue architecture plays a critical role.

1.2 Prostate Cancer

Approximately 240,000 men in the United States were diagnosed with prostate cancer in 2012 [2]. It remains the most commonly diagnosed cancer in U.S. men. While approximately 28,000 men died of prostate cancer in 2012, many patient's cancers are too small, low grade and noninvasive that they pose little risk to the life or health of the host. Identifying these patients is difficult with current diagnostic techniques. The best predictor of tumor risk to the patient is the biopsy with

consequent hematoxylin and eosin (H&E) analysis by a pathologist and Gleason scoring. However, as only a small fraction of the prostate is evaluated during a biopsy procedure, most physicians assume that the biopsy underestimates the extent of cancer and recommend more aggressive treatments [3]. This can result in overtreatment and potentially unnecessary side effects.

If diagnosed early and accurately though, prostate cancer can be very successfully treated with a radical prostatectomy. A significant challenge for the surgeon is to remove all cancerous tissue, while preserving the nerves surrounding the prostate that are responsible for continence and erectile function. These nerves, as well as the malignant glands, are too small to be visualized by eye. Intraoperative frozen sections (IFS) have been shown to provide some benefit in reducing positive surgical margins (PSMs) [4], however, they require time and, similar to diagnostic biopsies, only provide an assessment of a fraction of the area of interest. Further, as IFS requires the removal of tissue, there is always a risk of damaging the area one is trying to preserve.

As a result, radical prostatectomy has been estimated to have a 10 - 40% occurrence in PSMs [5–8] and 25 - 70% occurrence of postoperative impotence [9–13]. Thus, in both the diagnosis and in the treatment of prostate cancer a faster and more accurate way of characterizing the tissue at a cellular level could significantly improve treatment decision making and patient outcomes.

1.3 Multiphoton microscopy

Multiphoton microscopy [14] (MPM) has the potential to greatly improve upon the current standard for diagnosing and treating cancers. Several factors make it an ideal candidate as a valuable clinical imaging technology:

- MPM allows for real time histological tissue analysis at high resolution (< 1 μm);
- Deep imaging in thick specimens is possible for over 1 mm depth depending on the tissue [15];
- Images can be generated without contrast agent, based on inherent autofluorescence and harmonic generation [16];
- There is significantly reduced out of focus photobleaching and photodestruction as compared to fluorescence or confocal imaging;
- MPM simultaneously excites species that emit at different wavelengths.

MPM can be used to visualize similar tissue components as are visible in traditional histopathology. However MPM can produce these images in real time, in unstained and unfixed tissue [17–21], thus potentially allowing for faster diagnosis and intra-operative margin assessment. Table 1.1 details the types of tissue components that can be visualized using MPM and Table 1.2 and Figure 1.1 provide a comparison between multiphoton imaging and histology. The diagnostic capabilities of MPM have been successfully demonstrated in a variety of organs such as the gastrointestinal tract [17], the bladder [18], the lung [19], the ovaries [21], and the prostate [22].

Table 1.1 Tissue components visualized via Multiphoton Excitation of intrinsic emitters (reproduced from [23]).

Process	Source	Tissue Components Visualized	Ref.
2PE	NADH, Flavins, Retinol, Folic Acid	cell cytoplasm, striated muscle fibers (i.e., skeletal & cardiac muscles)	[20,24]
2PE	Elastin	elastic fibers (e.g., connective tissue, blood vessel walls)	[20]
3PE	Serotonin, Melatonin, Tyrosine, Tryptophan, 5-HIAA, 5-HTOL	cell cytoplasm, cell nuclei	[20]
SHG	Collagen	collagen fibers (e.g., connective tissue, blood vessel walls, components of neuronal tissue & muscle tissue)	[20,25–27]
SHG	Tubulin	Microtubules (e.g., cilia, mitotic spindles), cell cytoskeleton	[25,26,28]
SHG	Myosin	striated muscle fibers (i.e., skeletal & cardiac muscles)	[20,25–27,29]
THG	Myosin	striated muscle fibers (i.e., skeletal & cardiac muscles)	[25,27]
THG	Lipids & Lipid Bodies	neuronal tissue (e.g, axons, dentrites, myelin sheaths), cell cytoplasm	[25,30–32]
THG	Hemoglobin	RBCs, blood vessels	[25,27,30]
THG	Collagen	collagen fibers (e.g., connective tissue, blood vessel walls, components of neuronal tissue & muscle tissue)	[25,27]
THG	Elastin	elastic fibers (e.g., connective tissue, blood vessel walls)	[33]

Table 1.2 Tissue components visualized by histopathology & multiphoton excitation of intrinsic emitters (reproduced from [23]).

	Histopathological Stain	Multiphoton Process
Cell Nuclei	Hematoxylin, Masson's Trichome, Van Gieson, Iron Hematoxylin	Dark-appearing, no fluorescence
Cell Cytoplasm	Eosin, Masson's Trichome, Van Gieson,	2PE, 3PE
Collagen Fibers	Eosin, Masson's Trichome, Van Gieson, Periodic Acid-Schiff	SHG, THG
Elastic Fibers	Weigert's, Orcein's, Verhoeff's	2PE, THG
Striated Muscle	Hemotoxylin & Eosin, Masson's Trichome, Iron Hematoxylin	2PE, SHG, THG
Blood Cells	*RBC's:* Giesma, Eosin, Masson's Trichome, Iron Hematoxylin *WBC's:* Giesma, Hematoxylin & Eosin	THG (RBC's & WBC's)
Myelin	Hematoxylin & Eosin, Iron Hematoxylin	THG

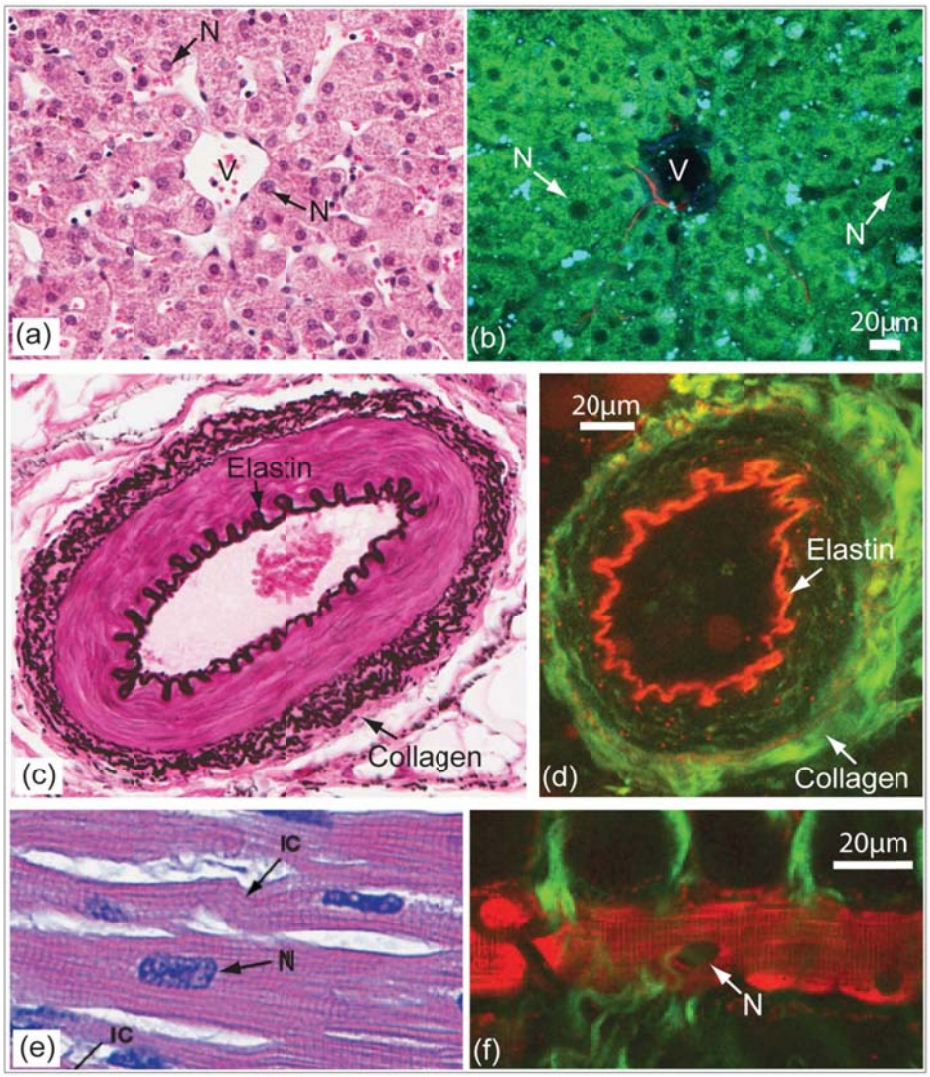

Figure 1.1: Common tissue components visualized via histology and multiphoton excitation of intrinsic emitters. (a, b) Comparison of cell nuclei & cytoplasm: liver hepatocytes radiating outward from a central vein (V). (a) H&E, the nuclei (N, blue) and cytoplasm (pink) of the hepatocytes are visible. (b) MPM, the nuclei (N) of the hepatocytes appear black (non-fluorescent), while the cytoplasm is brightly fluorescent via 2PE (green pseudocolor) [17]. (c, d) Elastin & collagen comparison: artery in cross-section, displaying characteristic layers of the artery wall. (c) Trichome w/Verhoeff's elastic stain, elastic fibers (black) and collagen fibers (pink) are visible. (d) MPM, 2PE of elastin (red pseudocolor) and SHG of collagen (green pseudocolor) are visible [20]. (e, f) Striated muscle comparison: longitudinal images of cardiac muscle cells, where the characteristic striations (i.e., vertical banding pattern) are visible. (e) H&E, the nuclei (N, blue) and extensive cytoplasm (pink) of the myocytes are visible [34]. (f) MPM, the nuclei (N, black) and extensive cytoplasm (2PE of NADH, red pseudocolor) of the myocytes are visible along with collagen connective tissue components (SHG, green pseudocolor) [20]. (Figure reproduced from [23]).

1.4 Multiphoton GRIN Endoscopy

A major challenge in translating multiphoton microscopy into a clinical setting is the limited penetration depth. As a result, an endoscopic approach is required. A number of different endoscopes and techniques have been demonstrated [35–46], including *in vivo* imaging of unstained tissues [47,48]. These devices are typically composed of a miniaturized scanning mechanism and focusing optics in a protective housing. The scanners proposed generally use either a miniaturized fiber scanning mechanism or microelectromechanical systems scanning mirror. The need to encapsulate a scanning mechanism into a housing of suitable size for minimally invasive procedures poses several challenges including: (1) uniformity of scan, (2) sensitivity, durability and reliability of the scanner, and (3) miniaturization of the distal scan mechanism and optics. A different approach has been to use gradient index (GRIN) lenses to relay the excitation light and TPF/SHG emission to and from an external microscope deep into soft tissue [49–53]. Since only the GRIN lens penetrates the tissue, the excitation, scanning, and collection optics need not be miniaturized for *in vivo* imaging. Another advantage of this approach is that GRIN lens systems, while rigid, can be fabricated in diameters as small as 0.350 mm.

In addition, GRIN lenses have been shown to be biocompatible and previously used in a clinical setting for non-penetrative imaging of chronic leg ulcers with delayed wound healing [54]. Use of a small diameter lens to penetrate deeply within tissue has been demonstrated with a hypodermic needle GRIN system [55] and in the study of sarcomere contractile dynamics in human muscle tissue [53]. These studies

show great promise for GRIN endoscopy to be used as either a guide for or a replacement of traditional surgical biopsies. Larger diameter (2 mm) GRIN lenses could also be used during traditional or minimally invasive surgery to assist the surgeon in tissue identification and margin assessment.

Previous studies, however, have been limited to short (<4 cm) GRIN systems primarily intended for small animals and external clinical use [53,54,56–59]. The eventual adaptation of GRIN lenses in the diagnosis of human diseases would require significantly longer GRIN endoscope systems. Commonly used prostate biopsy needles, for example, are as long as 25 cm. In this dissertation, we describe our efforts to develop a clinical multiphoton endoscope based on GRIN lens endoscopy. In Chapter 2, we demonstrate that multiphoton GRIN lens endoscopy is possible through long (>28cm) GRIN lens systems and describe our design and *in vivo* animal testing of a compact and portable multiphoton GRIN endoscope. In Chapter 3, we adapt our endoscope to show that its use is not limited to two photon imaging, but can be used as a three-photon endoscope also. Finally, in Chapter 4 we test the diagnostic capabilities of our endoscope using human *ex vivo* prostate tissue. Combined, these results show that multiphoton GRIN lens endoscopy has great potential to aid in the real time cellular assessment of unstained tissue *in vivo.* It could prove to be very helpful in guiding a diagnostic biopsy and providing a surgeon with valuable tissue information intra-operatively.

REFERENCES

1. R. Siegel, J. Ma, Z. Zou, and A. Jemal, "Cancer statistics, 2014.," CA. Cancer J. Clin. **64**, 9–29 (2014).

2. R. Siegel, D. Naishadham, and A. Jemal, "Cancer statistics, 2012.," CA. Cancer J. Clin. **62**, 10–29 (n.d.).

3. M. Noguchi, T. a Stamey, J. E. McNeal, and C. M. Yemoto, "Relationship between systematic biopsies and histological features of 222 radical prostatectomy specimens: lack of prediction of tumor significance for men with nonpalpable prostate cancer.," J. Urol. **166**, 104–9; discussion 109–10 (2001).

4. W. Dillenburg, V. Poulakis, U. Witzsch, R. de Vries, K. Skriapas, H.-M. Altmansberger, and E. Becht, "Laparoscopic radical prostatectomy: the value of intraoperative frozen sections.," Eur. Urol. **48**, 614–621 (2005).

5. R. C. Smith, a W. Partin, J. I. Epstein, and C. B. Brendler, "Extended followup of the influence of wide excision of the neurovascular bundle(s) on prognosis in men with clinically localized prostate cancer and extensive capsular perforation.," J. Urol. **156**, 454–7; discussion 457–8 (1996).

6. J. a Wieder and M. S. Soloway, "Incidence, etiology, location, prevention and treatment of positive surgical margins after radical prostatectomy for prostate cancer.," J. Urol. **160**, 299–315 (1998).

7. R. Watson, F. Civantos, and M. Soloway, "Positive surgical margins with radical prostatectomy: detailed pathological analysis and prognosis," Urology **5**, (1996).

8. M. Sofer, K. L. Hamilton-Nelson, J. J. Schlesselman, and M. S. Soloway, "Risk of positive margins and biochemical recurrence in relation to nerve-sparing radical prostatectomy.," J. Clin. Oncol. **20**, 1853–1858 (2002).

9. W. Bentas, M. Wolfram, J. Jones, R. Bräutigam, W. Kramer, and J. Binder, "Robotic Technology and the Translation of Open Radical Prostatectomy to Laparoscopy: The Early Frankfurt Experience with Robotic Radical Prostatectomy and One Year Follow-up," Eur. Urol. **44**, 175–181 (2003).

10. T. E. Ahlering, D. Skarecky, D. Lee, and R. V Clayman, "Successful transfer of open surgical skills to a laparoscopic environment using a robotic interface: initial experience with laparoscopic radical prostatectomy.," J. Urol. **170**, 1738–41 (2003).

11. C. Eden, D. Cahill, and J. Vass, "Laparoscopic radical prostatectomy: the initial UK series," BJU … 876–882 (2002).

12. J. Rassweiler and R. Marrero, "Transperitoneal laparoscopic radical prostatectomy: ascending technique," J. … **18**, (2004).

13. J. W. Saranchuk, M. W. Kattan, E. Elkin, a K. Touijer, P. T. Scardino, and J. a Eastham, "Achieving optimal outcomes after radical prostatectomy.," J. Clin. Oncol. **23**, 4146–51 (2005).

14. W. Denk, J. H. Strickler, and W. W. Webb, "Two-photon laser scanning fluorescence microscopy," Science (80-.). **248**, 73–6 (1990).

15. N. G. Horton, K. Wang, D. Kobat, C. G. Clark, F. W. Wise, C. B. Schaffer, and C. Xu, "In vivo three-photon microscopy of subcortical structures within an intact mouse brain," Nat. Photonics **7**, 205–209 (2013).

16. W. R. Zipfel, R. M. Williams, and W. W. Webb, "Nonlinear magic: multiphoton microscopy in the biosciences.," Nat. Biotechnol. **21**, 1369–77 (2003).

17. T. Makino, M. Jain, D. C. Montrose, A. Aggarwal, J. Sterling, B. P. Bosworth, J. W. Milsom, B. D. Robinson, M. M. Shevchuk, K. Kawaguchi, N. Zhang, C. M. Brown, D. R. Rivera, W. O. Williams, C. Xu, A. J. Dannenberg, and S. Mukherjee, "Multiphoton tomographic imaging: a potential optical biopsy tool for detecting gastrointestinal inflammation and neoplasia.," Cancer Prev. Res. (Phila). **5**, 1280–90 (2012).

18. M. Jain, B. D. Robinson, D. S. Scherr, J. Sterling, M.-M. Lee, J. Wysock, M. A. Rubin, F. R. Maxfield, W. R. Zipfel, W. W. Webb, and S. Mukherjee,

"Multiphoton microscopy in the evaluation of human bladder biopsies.," Arch. Pathol. Lab. Med. **136**, 517–26 (2012).

19. I. Pavlova, K. R. Hume, S. A. Yazinski, J. Flanders, T. L. Southard, R. S. Weiss, and W. W. Webb, "Multiphoton microscopy and microspectroscopy for diagnostics of inflammatory and neoplastic lung.," J. Biomed. Opt. **17**, 036014 (2012).

20. W. R. Zipfel, R. M. Williams, R. Christie, A. Y. Nikitin, B. T. Hyman, and W. W. Webb, "Live tissue intrinsic emission microscopy using multiphoton-excited native fluorescence and second harmonic generation.," Proc. Natl. Acad. Sci. U. S. A. **100**, 7075–80 (2003).

21. R. M. Williams, A. Flesken-Nikitin, L. H. Ellenson, D. C. Connolly, T. C. Hamilton, A. Y. Nikitin, and W. R. Zipfel, "Strategies for high-resolution imaging of epithelial ovarian cancer by laparoscopic nonlinear microscopy.," Transl. Oncol. **3**, 181–94 (2010).

22. A. K. Tewari, M. M. Shevchuk, J. Sterling, S. Grover, M. Herman, R. Yadav, K. Mudalair, A. Srivastava, M. A. Rubin, W. R. Zipfel, F. R. Maxfield, C. Xu, W. W. Webb, and S. Mukherjee, "Multiphoton microscopy for structure identification in human prostate and periprostatic tissue: implications in prostate cancer surgery.," BJU Int. **108**, 1421–9 (2011).

23. D. R. Rivera, "Multiphoton Endoscopy," Cornell University (2013).

24. S. Huang, A. A. Heikal, and W. W. Webb, "Two-photon fluorescence spectroscopy and microscopy of NAD(P)H and flavoprotein.," Biophys. J. **82**, 2811–25 (2002).

25. P. Friedl, K. Wolf, U. H. von Andrian, and G. Harms, "Biological second and third harmonic generation microscopy.," Curr. Protoc. Cell Biol. **Chapter 4**, Unit 4.15 (2007).

26. P. J. Campagnola, A. C. Millard, M. Terasaki, P. E. Hoppe, C. J. Malone, and W. A. Mohler, "Three-dimensional high-resolution second-harmonic generation imaging of endogenous structural proteins in biological tissues.," Biophys. J. **82**, 493–508 (2002).

27. M. Rehberg, F. Krombach, U. Pohl, and S. Dietzel, "Label-free 3D visualization of cellular and tissue structures in intact muscle with second and third harmonic generation microscopy.," PLoS One **6**, e28237 (2011).

28. D. A. Dombeck, K. A. Kasischke, H. D. Vishwasrao, M. Ingelsson, B. T. Hyman, and W. W. Webb, "Uniform polarity microtubule assemblies imaged in native brain tissue by second-harmonic generation microscopy.," Proc. Natl. Acad. Sci. U. S. A. **100**, 7081–6 (2003).

29. M. Both, M. Vogel, O. Friedrich, F. von Wegner, T. Künsting, R. H. A. Fink, and D. Uttenweiler, "Second harmonic imaging of intrinsic signals in muscle fibers in situ.," J. Biomed. Opt. **9**, 882–92 (n.d.).

30. S. Witte, A. Negrean, J. C. Lodder, C. P. J. de Kock, G. Testa Silva, H. D. Mansvelder, and M. Louise Groot, "Label-free live brain imaging and targeted patching with third-harmonic generation microscopy.," Proc. Natl. Acad. Sci. U. S. A. **108**, 5970–5 (2011).

31. D. Débarre, W. Supatto, A.-M. Pena, A. Fabre, T. Tordjmann, L. Combettes, M.-C. Schanne-Klein, and E. Beaurepaire, "Imaging lipid bodies in cells and tissues using third-harmonic generation microscopy.," Nat. Methods **3**, 47–53 (2006).

32. M. J. Farrar, F. W. Wise, J. R. Fetcho, and C. B. Schaffer, "In vivo imaging of myelin in the vertebrate central nervous system using third harmonic generation microscopy.," Biophys. J. **100**, 1362–71 (2011).

33. C.-K. Sun, C.-H. Yu, S.-P. Tai, C.-T. Kung, I.-J. Wang, H.-C. Yu, H.-J. Huang, W.-J. Lee, and Y.-F. Chan, "In vivo and ex vivo imaging of intra-tissue elastic fibers using third-harmonic-generation microscopy," Opt. Express **15**, 11167 (2007).

34. B. Young, J. S. Lowe, A. Stevens, and J. W. Heath, *Wheater's Functional Histology: A Text and Colour Atlas* (Churchhill Livingston Elsevier, 2006), p. 448.

35. F. Helmchen, M. S. Fee, D. W. Tank, and W. Denk, "A Miniature Head-Mounted Two-Photon Microscope," Neuron **31**, 903–912 (2001).

36. T. Wu, Z. Ding, K. Wang, M. Chen, and C. Wang, "Two-dimensional scanning realized by an asymmetry fiber cantilever driven by single piezo bender actuator for optical coherence tomography," Opt. Express **17**, 13819 (2009).

37. E. J. Seibel and Q. Y. J. Smithwick, "Unique features of optical scanning, single fiber endoscopy.," Lasers Surg. Med. **30**, 177–83 (2002).

38. M. T. Myaing, D. J. MacDonald, and X. Li, "Fiber-optic scanning two-photon fluorescence endoscope," Opt. Lett. **31**, 1076 (2006).

39. C. J. Engelbrecht, R. S. Johnston, E. J. Seibel, and F. Helmchen, "Ultra-compact fiber-optic two-photon microscope for functional fluorescence imaging in vivo," Opt. Express **16**, 5556 (2008).

40. Y. Wu, Y. Leng, J. Xi, and X. Li, "Scanning all-fiber-optic endomicroscopy system for 3D nonlinear optical imaging of biological tissues," Opt. Express **17**, 7907 (2009).

41. B. H. W. Hendriks, W. C. J. Bierhoff, J. J. L. Horikx, A. E. Desjardins, C. A. Hezemans, G. W. ’t Hooft, G. W. Lucassen, and N. Mihajlovic, "High-resolution resonant and nonresonant fiber-scanning confocal microscope.," J. Biomed. Opt. **16**, 026007 (2011).

42. J. Sawinski and W. Denk, "Miniature random-access fiber scanner for in vivo multiphoton imaging," J. Appl. Phys. **102**, 034701 (2007).

43. D. G. Ouzounov, D. R. Rivera, W. O. Williams, J. A. Stupinski, T. L. Southard, K. H. Hume, J. Bentley, R. S. Weiss, W. W. Webb, and C. Xu, "Dual modality endomicroscope with optical zoom capability.," Biomed. Opt. Express **4**, 1494–503 (2013).

44. D. R. Rivera, C. M. Brown, D. G. Ouzounov, I. Pavlova, D. Kobat, W. W. Webb, and C. Xu, "Compact and flexible raster scanning multiphoton endoscope capable of imaging unstained tissue.," Proc. Natl. Acad. Sci. U. S. A. **108**, 17598–603 (2011).

45. D. R. Rivera, C. M. Brown, D. G. Ouzounov, W. W. Webb, and C. Xu, "Multifocal multiphoton endoscope.," Opt. Lett. **37**, 1349–51 (2012).

46. D. R. Rivera, C. M. Brown, D. G. Ouzounov, W. W. Webb, and C. Xu, "Use of a lensed fiber for a large-field-of-view, high-resolution, fiber-scanning microendoscope.," Opt. Lett. **37**, 881–3 (2012).

47. M. Goetz, C. Fottner, E. Schirrmacher, P. Delaney, S. Gregor, C. Schneider, D. Strand, S. Kanzler, B. Memadathil, E. Weyand, M. Holtmann, R. Schirrmacher, M. M. Weber, M. Anlauf, G. Klöppel, M. Vieth, P. R. Galle, P. Bartenstein, M. F. Neurath, and R. Kiesslich, "In-vivo confocal real-time mini-microscopy in animal models of human inflammatory and neoplastic diseases.," Endoscopy **39**, 350–6 (2007).

48. C. M. Brown, D. R. Rivera, I. Pavlova, D. G. Ouzounov, W. O. Williams, S. Mohanan, W. W. Webb, and C. Xu, "In vivo imaging of unstained tissues using a compact and flexible multiphoton microendoscope.," J. Biomed. Opt. **17**, 040505 (2012).

49. R. Le Harzic, M. Weinigel, I. Riemann, K. König, and B. Messerschmidt, "Nonlinear optical endoscope based on a compact two axes piezo scanner and a miniature objective lens," Opt. Express **16**, 20588 (2008).

50. D. L. Dickensheets and G. S. Kino, "Micromachined scanning confocal optical microscope," Opt. Lett. **21**, 764 (1996).

51. U. Hofmann, S. Muehlmann, M. Witt, K. Doerschel, R. Schuetz, and B. Wagner, "<title>Electrostatically driven micromirrors for a miniaturized confocal laser scanning microscope</title>," in *Symposium on Micromachining and Microfabrication*, M. E. Motamedi and R. Goering, eds. (International Society for Optics and Photonics, 1999), pp. 29–38.

52. W. Piyawattanametha, E. D. Cocker, L. D. Burns, R. P. Barretto, J. C. Jung, H. Ra, O. Solgaard, and M. J. Schnitzer, "In vivo brain imaging using a portable 2.9 g two-photon microscope based on a microelectromechanical systems scanning mirror.," Opt. Lett. **34**, 2309–11 (2009).

53. M. E. Llewellyn, R. P. J. Barretto, S. L. Delp, and M. J. Schnitzer, "Minimally invasive high-speed imaging of sarcomere contractile dynamics in mice and humans.," Nature **454**, 784–8 (2008).

54. K. König, A. Ehlers, I. Riemann, S. Schenkl, R. Bückle, and M. Kaatz, "Clinical two-photon microendoscopy.," Microsc. Res. Tech. **70**, 398–402 (2007).

55. R. S. Pillai, D. Lorenser, and D. D. Sampson, "Deep-tissue access with confocal fluorescence microendoscopy through hypodermic needles.," Opt. Express **19**, 7213–21 (2011).

56. B. A. Flusberg, J. C. Jung, E. D. Cocker, E. P. Anderson, and M. J. Schnitzer, "In vivo brain imaging using a portable 3.9 gram two-photon fluorescence microendoscope," Opt. Lett. **30**, 2272 (2005).

57. M. J. Levene, D. A. Dombeck, K. A. Kasischke, R. P. Molloy, and W. W. Webb, "In vivo multiphoton microscopy of deep brain tissue.," J. Neurophysiol. **91**, 1908–12 (2004).

58. J. C. Jung, A. D. Mehta, E. Aksay, R. Stepnoski, and M. J. Schnitzer, "In vivo mammalian brain imaging using one- and two-photon fluorescence microendoscopy.," J. Neurophysiol. **92**, 3121–33 (2004).

59. J. C. Jung and M. J. Schnitzer, "Multiphoton endoscopy," Opt. Lett. **28**, 902 (2003).

CHAPTER 2

IN VIVO IMAGING OF UNSTAINED TISSUES USING LONG GRADIENT INDEX LENS MULTIPHOTON ENDOSCOPIC SYSTEMS[1]

Abstract

We characterize long (up to 285 mm) gradient index (GRIN) lens endoscope systems for multiphoton imaging. We fabricate a portable, rigid endoscope system suitable for imaging unstained tissues, potentially deep within the body, using a GRIN lens system of 1 mm diameter and 8 cm length. The portable device is capable of imaging a ~200 μm diameter field of view at 4 frames/s. The lateral and axial resolution in water is 0.85 μm and 7.4 μm respectively. In vivo images of unstained tissues in live, anesthetized rats using the portable device are presented. These results show great promise for GRIN endoscopy to be used clinically.

2.1 Introduction

Two-photon fluorescence (TPF) and second-harmonic generation (SHG) microscopy are powerful tools for imaging unstained biological tissues [1]. These label-free techniques are capable of producing high-resolution real-time in vivo images and have shown great promise for medical diagnostics of various diseases, potentially replacing surgical biopsies [2–7]. The maximum imaging depth, however, is limited in most tissues to ~1 mm [8,9].

[1] The contents of this chapter have been reproduced from Biomedical Optics Express, Vol. 3, No. 5, pp. 1077-1085, 2012.

One strategy to overcome the depth limitation is to develop miniaturized TPF microscopes that could be used as endoscopes in a clinical setting. A number of different endoscopes and techniques have been demonstrated [10–17], including in vivo imaging of unstained tissues [18]. These devices are typically composed of a miniaturized scanning mechanism and focusing optics in a protective housing. The scanners proposed generally use either a miniaturized fiber scanning mechanism or microelectromechanical systems scanning mirror. The need to encapsulate a scanning mechanism into a housing of suitable size for minimally invasive procedures poses several challenges including: (1) uniformity of scan, (2) sensitivity, durability and reliability of the scanner, and (3) miniaturization of the distal scan mechanism and optics. A different approach has been to use gradient index (GRIN) lenses to relay the excitation light and TPF/SHG emission to and from an external microscope deep into soft tissue [19–22]. Since only the GRIN lens penetrates the tissue, the excitation, scanning, and collection optics need not be miniaturized for in vivo imaging. GRIN lenses have been shown to be biocompatible and previously used in a clinical setting for non-penetrative imaging of chronic leg ulcers with delayed wound healing [23]. Use of a small diameter lens to penetrate deeply within tissue has been demonstrated with a hypodermic needle GRIN system [24]. These studies show great promise for GRIN endoscopy to be used as either a guide for or a replacement of traditional surgical biopsies.

Previous studies, however, have been limited to short (<4 cm) GRIN systems primarily intended for small animals and external clinical use [19–23]. The eventual adaptation of GRIN lenses in the diagnosis of human diseases would require

significantly longer GRIN endoscope systems. Commonly used prostate biopsy needles, for example, are as long as 25 cm. In this study we investigate the effect of GRIN system length on the imaging performance. We characterize the loss in imaging performance with increased GRIN system length and present a compact and portable two-photon microscope that could be used in a clinical environment in combination with various GRIN lens systems. Finally, the capability of the system for in vivo imaging of unstained tissues is demonstrated in live, anesthetized rats.

2.2 GRIN endoscopes

GRIN lenses use a negative gradient in the refractive index of glass with increasing radius to bend and focus light. The pitch of a GRIN lens characterizes how many internal images are formed within the lens, with a pitch of 1 being the length of one full sinusoidal path. Most previously reported GRIN two-photon endoscope systems use a combination of relay and objective GRIN lenses in either a doublet (relay/objective) or triplet (objective/relay/objective) system [19–23]. The usually low NA relay lens avoids a tight focus of the excitation light within the glass, while the higher NA objective lens allows for high-resolution two-photon imaging at the sample. Previous studies have shown that a doublet system offers several advantages over a triplet system such as similar fields of view at reduced lens cost, greater image magnification, lower NA for coupling the laser beam, and lower autofluorescence at the endoscope surface [21]. GRIN lenses are commercially available in varying lengths and in diameters as small as 350 μm. We obtained doublet systems of 1 mm and 2 mm diameter from GRINTECH GmbH consisting of a 0.5 NA objective lens

and a 0.1 NA relay lens of varying length and pitch. The different systems obtained are summarized in Table 2.1. All systems were designed for 800 nm excitation light and with working distances of 100-140 μm in air on either side (~140-190 μm in water). The GRIN lens systems were protected by a stainless steel tube of 0.1 mm thickness, resulting in total system outer diameters (OD) of 1.2 mm and 2.2 mm.

Table 2.1. Summary of Optical Characterization Results[a]

GRIN System	Part Number	Diameter (mm)	Length (mm)	Relay Lens Pitch	FWHM (μm)		Diameter of FOV (μm)
					Lateral	Axial	
1A	GT-ERLS-100-075-11-50-NC	1.00	35.9	0.75	0.94	10.8	199
1B	GT-ERLS-100-125-11-50-NC	1.00	57.7	1.25	0.99	15.1	195
2A	GT-ERLS-200-075-11-50-NC	2.00	81.4	0.75	0.99	12.6	370
2B	GT-ERLS-200-125-11-50-NC	2.00	132.6	1.25	1.05	15.6	365
2C	GT-ERLS-200-275-11-50-NC	2.00	285.0	2.75	1.17	25.0	359

[a] Six different doublet grin systems were designed by and purchased from Grintech GmbH. The lateral and axial two-photon resolution were determined in air using subresolution fluorescent beads and a thin rhodamine film respectively.

2.3. Experimental setup

Figure 2.1 shows the custom built horizontal multiphoton microscope used to characterize the GRIN lens systems. A mode-locked Ti:sapphire laser (Tsunami, Spectra Physics, Inc.) was used as the excitation source at 800 nm with 10 nm bandwidth. Dual axis (5 mm diameter) galvo based scan mirrors (GVSM002, Thorlabs Inc.), and two scan lenses of 10 cm and 30 cm focal length (respectively, AC508-100-B-ML and AC508-300-B-ML, Thorlabs Inc.) were used to scan the beam angle at the overfilled back aperture of a 0.1 NA microscope objective. The focus of the objective was raster scanned by the galvo mirrors across the proximal face of the GRIN lens systems. The GRIN lens systems were mounted on a three axis manual linear

translational stage close to the focal plane of the objective to aid alignment. All optical characterizations were conducted by moving the sample mounted on a 3D stage (MP-285, Sutter Instruments) allowing axial scanning of the sample while maintaining the GRIN lens system in a fixed position. The fluorescent signal from the sample was epi-collected through the GRIN lenses and the microscope objective. Collected light is reflected by a dichroic beam splitter (FF-665-Di01, Semrock Inc.). After passing through two 575/250 bandpass filters (HQ575_250 2p, Chroma Technology Corp.) separated by a colored glass (FGS900, Thorlabs Inc.), the fluorescence is detected by a photo-multiplier tube (PMT) (HC125-02, Hamamatsu Photonics). Data acquisition and motion control were implemented using a DAQ card (PCI-6115, National Instruments Corp.) and MPScan software [25]. The axial resolution of the GRIN lens systems was characterized in air using the full width at half maximum (FWHM) two-photon excited fluorescence signal from a 500 nm thin film of Rhodamine B (RhB) dye, while the lateral resolution was characterized using FWHM two-photon excited fluorescence from subresolution (0.2 μm) fluorescent beads. The field of view (FOV) was characterized by raster-scanning the proximal face of the GRIN lens system and measuring the one-photon transmission using a photodiode (SM05PD1A, Thorlabs Inc.), and was defined as the FWHM of the resulting intensity profile.

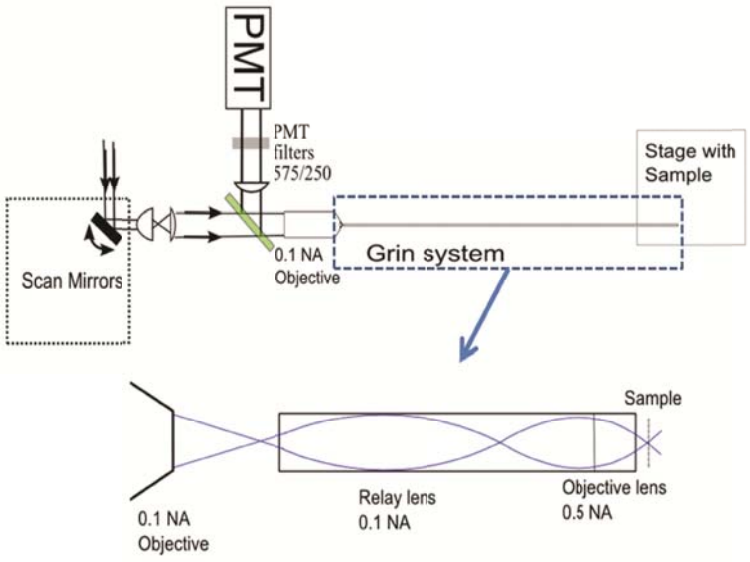

Figure 2.1. Experimental setup used for the optical characterization of the long gradient index endoscope systems and close-up of the doublet grin system design (shown here using a 0.75 relay lens pitch).

2.4. GRIN endoscope characterization

The on-axis lateral and axial resolutions and FOV of the systems are summarized in Table 2.1. Figure 2.2 shows the beam profile along the axial and lateral directions of the longest GRIN system (2C). Increasing the length of the relay lens results in only a small deterioration of the lateral resolution. The axial resolution declines more significantly for the longer systems. We believe that this is mainly due to increased accumulation of spherical aberrations, as can be seen by the asymmetric thin film response curve in Figure 2.2(b). These characterizations were done in air; we would expect the axial resolution scaled by a factor of ~1.3 in tissue. Nevertheless, axial resolution remains on the order of one layer of mammalian cells for all of

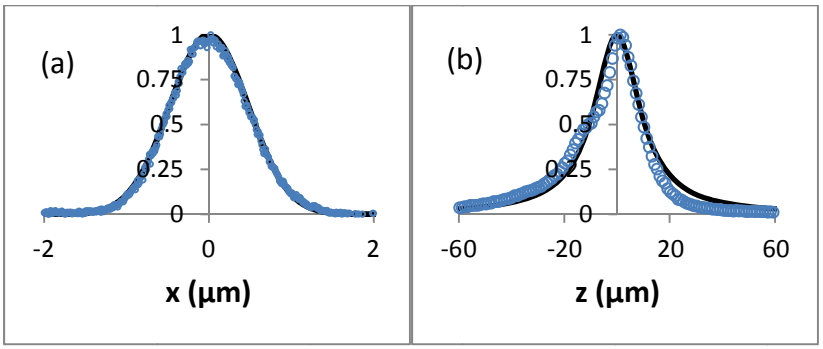

Figure 2.2. Two-photon lateral and axial resolution of GRIN system 2C (285 mm length). (a) Lateral intensity line profile across a subresolution fluorescent bead. (b) Axial intensity profile across a thin film rhodamine slide.

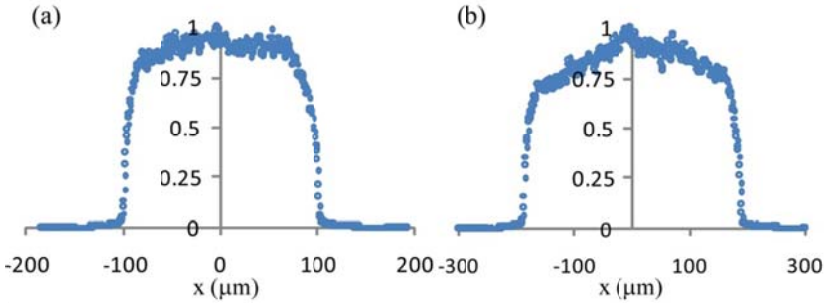

Figure 2.3. Normalized one photon transmission intensity across the field of view for (a) GRIN system 1B and (b) GRIN system 2C.

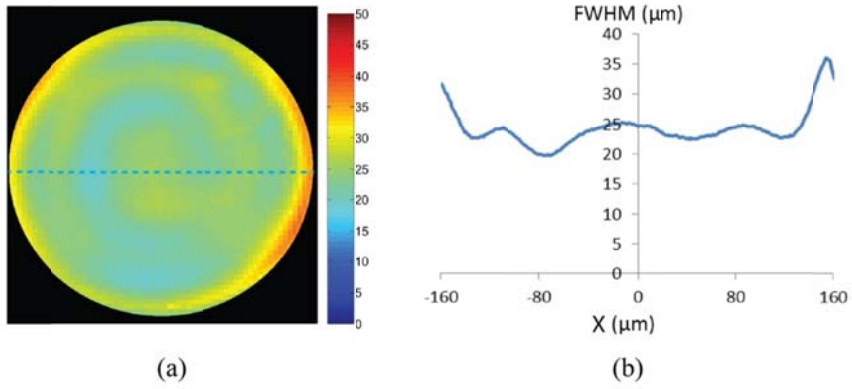

Figure 2.4. Off-axis performance. Axial FWHM in µm plotted across the FOV of GRIN system 2C (285 mm length).

the GRIN lenses tested. The FOV for all systems (195-370 µm) is relatively large for the small OD systems. Figure 2.3 shows the most and least uniform intensity curves obtained from the transmission imaging (GRIN system 1B and 2C respectively).

The off-axis axial resolutions of the different systems were measured by acquiring a through-focus z-series of the RhB thin film and fitting a Lorentzian function to individual off-axis areas of ~6 by 6 μm in size. The resulting FWHM of each area is plotted in Figure 2.4. The lateral off-axis performance was also measured for system 1B using sub-resolution fluorescent beads, and the FWHM of the obtained PSF remained below 1.2 μm up to the edge of the FOV. These results indicate that the off-axis resolution of these GRIN systems remains within ~20% of the on-axis resolution for most of the FOV (~80% of the area). The ability to deliver ultrashort pulses to the sample is critically important for multiphoton imaging. The effect of the longest GRIN lens system (285 mm in length, system 2C) on the excitation laser pulse was characterized. Without dispersion compensation, the initial 80 fs pulse width was broadened to 740 fs. Using precompensation with a rotating cylindrical lens and grating [26], we were able to achieve an 85 fs pulse width at the sample, indicating that a simple dispersion compensation setup that accounts for the second order dispersion is sufficient for delivering pulses on the order of 80 fs.

2.5. Portable endoscope design and system characterization

To demonstrate that these GRIN lens systems have potential clinical applications, a compact, fiber-coupled multiphoton GRIN lens endoscope was constructed for in vivo image acquisition (Figure 2.5). The 800 nm femtosecond pulse from the Ti:sapphire laser is delivered by a 2 meter hollow core PCF fiber (HC-800B, Thorlabs Inc.), and collimated to a beam of about 2 mm diameter using an aspheric

lens. A small aperture (3 mm) galvo scanning mirror system (6210H, Cambridge Technology) was selected for a fast imaging rate (up to 4 frames/s at 512 by 512 pixels). The beam is then expanded by two scan lenses of 18 and 36 mm focal length (respectively, LSM02-BB and LSM03-BB, Thorlabs Inc.) to underfill a 0.3 NA microscope objective (RMS10X-PF, Thorlabs Inc.) to achieve an effective NA of ~0.1. The microscope objective couples the excitation beam into the proximal side of the GRIN lens system. We selected the longest 1 mm diameter system (1B) for this demonstration. The fluorescence signal from the sample is epi-collected through the GRIN lenses and the objective, and is reflected by a dichroic beam splitter (FF705-Di01, Semrock Inc.). After passing through two short pass filters (FF01-720/SP, Semrock Inc.) separated by colored glass (FGS900, Thorlabs Inc.), a second dichroic (Di01-R405, Semrock Inc.) separated the signal into the second harmonic and the autofluorescence channel. The housing of the GRIN lens endoscope was constructed from custom machined aluminum components using a milling machine with a fabrication tolerance of 0.001". Optical elements in the GRIN endoscope were aligned in the z-axis to specification using calipers. We verified that illumination light projected through the system was centered as it passed through each optical element. The GRIN lens position was verified by confirming the focal length of the lens met specification (i.e. verified GRIN lens working distance by locating peak two-photon excited signal of a fluorescent sample ~130μm

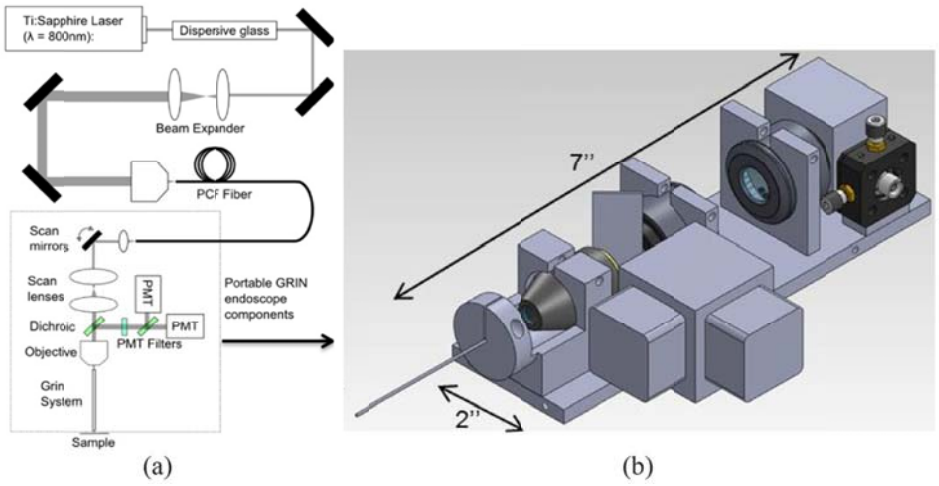

Figure 2.5. Portable GRIN endoscope. (a) Optical drawing and (b) Solidworks drawing of the GRIN based endoscope system. Total system length of the portable device is 10.6'' (including GRIN system).

from the lens using a three-axis micrometer). The hollow core fiber has anomalous dispersion at 800 nm. This allowed us to precompensate the dispersion of the fiber and the GRIN lens by using a 10 cm rod of dispersive SF10 glass in the beam path before coupling into the fiber, resulting in a ~120 fs pulse width at the sample. The axial resolution of the GRIN lens endoscope system is 6.5 μm FWHM in air and 7.4 μm FWHM in water, measured using the RhB thin film as described above. The measured lateral resolution in both air and water is 0.85 μm FWHM using sub-resolution beads.

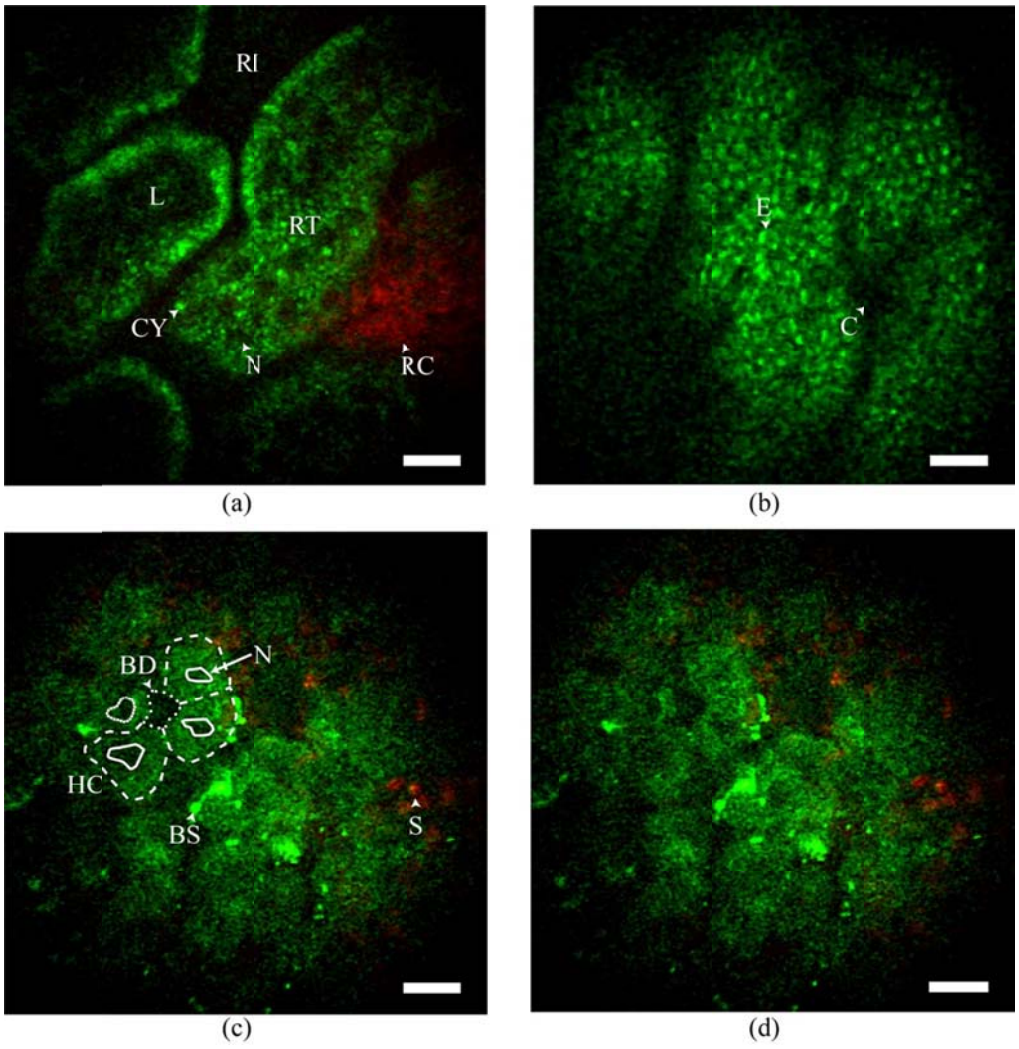

Figure 2.6. Unaveraged *in vivo* images of unstained rat tissue. The pseudo-color images show red SHG signal (<405 nm) and green intrinsic fluorescent emission (405-700 nm). (a) Image of the superficial kidney renal cortex shows dark renal interstitium (RI), dark cellular nuclei (N) and bright intrinsic fluorescent cytoplasm (CY) that form the epithelial cells in the renal tubules (RT), SHG signal from the tough fibrous layer that forms the renal capsule (RC), and the dark blood filled lumen (L) inside the renal tubules. (b) Image of the inner colon wall shows bright intrinsic fluorescent signal from enterocytes (E) surrounding dark circular crypts (C). (c) Image of the rat liver showing ~ 20 μm diameter hepatocytes (coarse dashed line) with dark nuclei (N, solid line) chained together to form hepatic chords (HC), a dark bile duct (BD, fine dashed line) and bright intrinsically fluorescent bile salts (BS), as well as SHG emission from the septa (S) a fibrous tissue bands that separates hepatocyte nodules. (d) Image of the rat liver without labels shown for clarity. In these images, scale bars are 20 μm.

Note! After publication of this paper, questions have been raised about whether the bright structures labeled as BS are actually bile salts. While the abbreviation may be very accurate, the label in this figure may be inaccurate in indicating bile salts!

2.7. Discussion

Both the axial and lateral resolution obtained for our systems (1A, 1B, 2A, and 2B) are similar to previous reports of similar NA systems at much shorter lengths [19, 20, 22, 23]. Our longest system, 2C, shows a significant degradation in axial resolution. This is probably due to the accumulation of spherical aberrations and manufacturing imperfections with increasing relay lens length. The lateral resolution, however, is only minimally affected, and the axial resolution remains on the order of a layer of mammalian cells, showing promise that long GRIN endoscopy has diagnostic potential. This is also evident from our in vivo imaging results. While image quality is decreased slightly when compared to a microscope objective of similar NA, many of the important tissue features are identifiable, show similarity to anatomic features seen in histology slides, and are potentially useful for diagnosis [27]. It is also noteworthy that no tissue damage was observed throughout the in vivo experiments, and our imaging conditions were comparable to those previously shown to have negligible tissue mutagenicity [28, 29]. In our imaging experiments, using up to 75mW illumination power at the sample, we did not witness any laser-induced visible luminescence within the GRIN endoscope, a concern with increasing relay lens length due to the increased number of internal foci. Previous studies have found this effect in higher NA systems (0.45 NA) with a threshold of 73 mW at 800nm [23]. We did observe, however, when the GRIN lens was misaligned to the extent that the distal focus was inside the high NA GRIN objective lens, the endoscope probe was damaged. The FOV for all systems remained large enough for diagnostic potential (195-370 μm diameter).

While long GRIN lens systems are limited to rigid endoscope applications, they offer several advantages over flexible multiphoton endoscopes. A significant advantage is the diameter of the endoscope probe. GRIN lenses are commercially available in diameters as small as 350 μm, which allows them to be inserted into needles as small as 22 gauge (inner diameter of 413 μm). Using the doublet design, we would expect similar imaging performance with such a lens except with a smaller FOV of about 70 μm diameter. Furthermore, the use of externally mounted galvo based scanning mirrors solves several challenges faced by other endoscope designs when considering clinical implementation such as uniformity of the scan and durability of the device. Because GRIN lenses are inexpensive, they could ultimately be used as disposable devices, eliminating the need for sterilizing the endoscope probe between procedures. The GRIN lens approach would also allow for an external focus adjustment in the depth of the sample without movement of the endoscope probe that has penetrated the tissue. By axially translating the scan objective, a z-scan in the sample of 0 to 95 μm from the surface of the lens has previously been shown [20].

2.8. Conclusions

We have demonstrated that TPF and SHG imaging are possible through long GRIN lens systems up to 28.5 cm in length. Long GRIN lenses can be integrated with a compact and portable two-photon microscope suitable for a clinical environment. The device presented can acquire TPF and SHG images at a rate of 4 frames/s with a field of view of ~200 μm diameter and with subcellular resolution. The presented in

vivo results of unstained organs of live rats show great promise for using GRIN endoscopy for optical biopsy.

Acknowledgments

This research was made possible by Grant Number R01-CA133148, from the National Institutes of Health/National Cancer Institute and Grant Number R01-EB006736, "Development of Medical Multiphoton Microscopic Endoscopy" from the National Institutes of Health/National Institute of Biomedical Imaging and Bioengineering. We thank members of the Xu and Webb research groups as well as Dr. Douglas Scherr and Dr. Sushmita Mukherjee of Weill Cornell Medical College for discussions and technical suggestions. We also thank Dr. Wendy Williams of the Cornell Center for Animal Resources and Education for her assistance with the in vivo imaging experiments and Mr. Herbert Stürmer of GRINTECH GmbH for discussions and technical suggestions.

REFERENCES

1. W. Denk, J. H. Strickler, and W. W. Webb, “Two-photon laser scanning fluorescence microscopy,” Science 248(4951), 73–76 (1990).

2. S. J. Lin, S. H. Jee, C. J. Kuo, R. J. Wu, W. C. Lin, J. S. Chen, Y. H. Liao, C. J. Hsu, T. F. Tsai, Y. F. Chen, and C. Y. Dong, “Discrimination of basal cell carcinoma from normal dermal stroma by quantitative multiphoton imaging,” Opt. Lett. 31(18), 2756–2758 (2006).

3. S. Mukherjee, J. S. Wysock, C. K. Ng, M. Akhtar, S. Perner, M. M. Lee, M. A. Rubin, F. R. Maxfield, W. W. Webb, and D. S. Scherr, “Human bladder cancer diagnosis using Multiphoton microscopy,” Proc. SPIE 7161, 716117, 716117-10 (2009).

4. I. Pavlova, K. R. Hume, S. A. Yazinski, J. Flanders, T. L. Southard, R. S. Weiss, and W. W. Webb, “Multiphoton microscopy and microspectroscopy for diagnostics of inflammatory and neoplastic lung,” J. Biomed. Opt. 17(3), 036014 (2012).

5. M. C. Skala, J. M. Squirrell, K. M. Vrotsos, J. C. Eickhoff, A. Gendron-Fitzpatrick, K. W. Eliceiri, and N. Ramanujam, “Multiphoton microscopy of endogenous fluorescence differentiates normal, precancerous, and cancerous squamous epithelial tissues,” Cancer Res. 65(4), 1180–1186 (2005).

6. C. C. Wang, F. C. Li, R. J. Wu, V. A. Hovhannisyan, W. C. Lin, S. J. Lin, P. T. So, and C. Y. Dong, "Differentiation of normal and cancerous lung tissues by multiphoton imaging," J. Biomed. Opt. 14(4), 044034 (2009).

7. P. Wilder-Smith, K. Osann, N. Hanna, N. El Abbadi, M. Brenner, D. Messadi, and T. Krasieva, "In vivo multiphoton fluorescence imaging: a novel approach to oral malignancy," Lasers Surg. Med. 35(2), 96–103 (2004).

8. D. Kobat, M. E. Durst, N. Nishimura, A. W. Wong, C. B. Schaffer, and C. Xu, "Deep tissue multiphoton microscopy using longer wavelength excitation," Opt. Express 17(16), 13354–13364 (2009).

9. D. Kobat, N. G. Horton, and C. Xu, "In vivo two-photon microscopy to 1.6-mm depth in mouse cortex," J. Biomed. Opt. 16(10), 106014 (2011).

10. L. Fu, A. Jain, C. Cranfield, H. Xie, and M. Gu, "Three-dimensional nonlinear optical endoscopy," J. Biomed. Opt. 12(4), 040501 (2007).

11. M. T. Myaing, D. J. MacDonald, and X. Li, "Fiber-optic scanning two-photon fluorescence endoscope," Opt. Lett. 31(8), 1076–1078 (2006).

12. D. R. Rivera, C. M. Brown, D. G. Ouzounov, I. Pavlova, D. Kobat, W. W. Webb, and C. Xu, "Compact and flexible raster scanning multiphoton endoscope capable of imaging unstained tissue," Proc. Natl. Acad. Sci. U.S.A. 108(43), 17598–17603 (2011).

13. S. Tang, W. Jung, D. McCormick, T. Xie, J. Su, Y. C. Ahn, B. J. Tromberg, and Z. Chen, “Design and implementation of fiber-based multiphoton endoscopy with microelectromechanical systems scanning,” J. Biomed. Opt. 14(3), 034005 (2009).

14. Y. Wu, Y. Leng, J. Xi, and X. Li, “Scanning all-fiber-optic endomicroscopy system for 3D nonlinear optical imaging of biological tissues,” Opt. Express 17(10), 7907–7915 (2009).

15. E. J. Seibel and Q. Y. Smithwick, “Unique features of optical scanning, single fiber endoscopy,” Lasers Surg. Med. 30(3), 177–183 (2002).

16. D. R. Rivera, C. M. Brown, D. G. Ouzounov, W. W. Webb, and C. Xu, “Use of a lensed fiber for a large-field-of-view, high-resolution, fiber-scanning microendoscope,” Opt. Lett. 37(5), 881–883 (2012).

17. D. R. Rivera, C. M. Brown, D. G. Ouzounov, W. W. Webb, and C. Xu, “Multifocal multiphoton endoscope,” Opt. Lett. 37(8), 1349–1351 (2012).

18. C. M. Brown, D. R. Rivera, I. Pavlova, D. G. Ouzounov, W. O. Williams, S. Mohanan, W. W. Webb, and C. Xu, “In vivo imaging of unstained tissues using a compact and flexible multiphoton microendoscope,” J. Biomed. Opt. 17(4), 040505 (2012).

19. B. A. Flusberg, J. C. Jung, E. D. Cocker, E. P. Anderson, and M. J. Schnitzer, “In vivo brain imaging using a portable 3.9 gram two-photon fluorescence microendoscope,” Opt. Lett. 30(17), 2272–2274 (2005).

20. M. J. Levene, D. A. Dombeck, K. A. Kasischke, R. P. Molloy, and W. W. Webb, “In vivo multiphoton microscopy of deep brain tissue,” J. Neurophysiol. 91(4), 1908–1912 (2004).

21. J. C. Jung, A. D. Mehta, E. Aksay, R. Stepnoski, and M. J. Schnitzer, “In vivo mammalian brain imaging using one- and two-photon fluorescence microendoscopy,” J. Neurophysiol. 92(5), 3121–3133 (2004).

22. J. C. Jung and M. J. Schnitzer, “Multiphoton endoscopy,” Opt. Lett. 28(11), 902–904 (2003).

23. K. König, A. Ehlers, I. Riemann, S. Schenkl, R. Bückle, and M. Kaatz, “Clinical two-photon microendoscopy,” Microsc. Res. Tech. 70(5), 398–402 (2007).

24. R. S. Pillai, D. Lorenser, and D. D. Sampson, “Deep-tissue access with confocal fluorescence microendoscopy through hypodermic needles,” Opt. Express 19(8), 7213–7221 (2011).

25. Q. T. Nguyen, P. S. Tsai, and D. Kleinfeld, “MPScope: a versatile software suite for multiphoton microscopy,” J. Neurosci. Methods 156(1-2), 351–359 (2006).

26. M. E. Durst, D. Kobat, and C. Xu, “Tunable dispersion compensation by a rotating cylindrical lens,” Opt. Lett. 34(8), 1195–1197 (2009).

27. L. P. Gartner and J. L. Hiatt, Color Textbook of Histology (W.B. Saunders, Philadelphia, 2001).

28. J. M. Dela Cruz, J. D. McMullen, R. M. Williams, and W. R. Zipfel, "Feasibility of using multiphoton excited tissue autofluorescence for in vivo human histopathology," Biomed. Opt. Express 1(5), 1320–1330 (2010).

29. R. Ramasamy, J. Sterling, E. S. Fisher, P. S. Li, M. Jain, B. D. Robinson, M. Shevchuck, D. Huland, C. Xu, S. Mukherjee, and P. N. Schlegel, "Identification of spermatogenesis with multiphoton microscopy: an evaluation in a rodent model," J. Urol. 186(6), 2487–2492 (2011).

CHAPTER 3

THREE-PHOTON EXCITED FLUORESCENCE IMAGING OF UNSTAINED TISSUE USING A GRIN LENS ENDOSCOPE[2]

Abstract

We present a compact and portable three-photon gradient index (GRIN) lens endoscope system suitable for imaging of unstained tissues, potentially deep within the body, using a GRIN lens system of 1 mm diameter and 8 cm length. The lateral and axial resolution in water is 1.0 μm and 9.5 μm, respectively. The ~200 μm diameter field of view is imaged at 2 frames/s using a fiber-based excitation source at 1040 nm. Ex vivo imaging is demonstrated with unstained mouse lung at 5.9 mW average power. These results demonstrate the feasibility of three-photon GRIN lens endoscopy for optical biopsy.

3.1. Introduction

In vivo two-photon (2P) microscopy has become a valuable tool for the study of subsurface features in intact tissues and organs [1]. To be clinically useful, endoscopic 2P approaches are required. A number of different endoscopes and techniques have been demonstrated in the past [2–9], including *in vivo* imaging of unstained tissues [10,11].

[2] The contents of this chapter have been reproduced from Biomedical Optics Express, Vol. 4, No. 5, pp. 652-658, 2013.

Previous 2P endoscope demonstrations rely on the mode-locked Ti:S laser at 800 nm to excite intrinsic fluorescence. However, longer excitation wavelengths have been shown to provide several advantages. As a result of an increased scattering length in tissue for longer excitation sources, the imaging penetration depth can be increased significantly using longer excitation wavelengths [12,13]. There are also strong indications that using longer wavelengths could lead to diminished phototoxicity. For example, imaging with longer wavelength has been shown to reduce destructive plasma formation [14,15]. Furthermore, femtosecond pulsed excitation at 1030 to 1070 nm can be conveniently provided by robust, compact fiber based lasers, which will significantly reduce the cost and improve the clinical compatibility. Although fiber lasers at these wavelengths can be used for 2P imaging of red dyes [16], 2P excitation of intrinsic molecules such as nicotinamide adenine dinucleotide (NADH) and flavin adenine dinucleotide (FAD) is impractical using the fiber source due to their small 2P cross sections at the long wavelengths [17].

Three-photon (3P) microscopy was first demonstrated in the 1990s [17–19]. 3P excitation is an effective approach to extend the spectral range of the excitation source. For example, 3P intrinsic fluorescence microscopy has been performed with deep UV-excitable intrinsic fluorophores such as serotonin and melatonin [20,21]. Here we demonstrate a GRIN lens endoscope that is capable of imaging unstained mouse lung tissues using 3P excitation by a fiber laser at 1040 nm. To the best of our knowledge, this is the first demonstration of 3P imaging of unstained tissues through a compact and portable system with potential for endoscopic tissue diagnosis.

3.2. Endoscope design and characterization

The compact and portable GRIN lens endoscope is shown in Figure 3.1, which was described in our previous work for 2P excitation of intrinsic fluorescence using a mode-locked Ti:S laser at 800 nm [11]. This system weighs less than 2lbs and was used successfully for *in vivo* 2P imaging in rats. For 3P endoscopic imaging, we used a longer wavelength, fiber laser source. (IMRA μJewel laser, 1040 nm wavelength and 1 MHz repetition rate). The optical components such as scan mirrors, scan lenses, objective and GRIN lens system are compatible with this new excitation source. For example, we found that the transmission of the GRIN lens is ~ 80% at 1040 nm, which is adequate for our applications. Modifications were made in the pulse delivery. The excitation light is delivered to the endoscope via a 1.6 m long hollow-core photonic band-gap fiber (HC-1060-2, NKT Photonics). A half-wave plate (WPH05M-1053, Thorlabs Inc.) was used to align the polarization of the excitation light with the polarization axis of the fiber. An aspheric lens on the portable GRIN lens endoscope collimates the excitation light to a beam about 2 mm in diameter. A small aperture (3 mm), galvanometer scanning mirror system (6210H, Cambridge Technology) allows for a fast imaging rate (up to 4 frames/s at 512 by 512 pixels). The beam is then expanded by two scan lenses 18 and 36 mm in focal length (respectively, LSM02-BB and LSM03-BB, Thorlabs Inc.) to underfill a 0.3 NA microscope objective (RMS10X-PF, Thorlabs Inc.) to achieve an effective focusing NA of ~0.1. A polarizer was added between the scan lenses to eliminate any residual light in the orthogonal polarization. The microscope objective couples the excitation beam into the proximal side of the GRIN lens system. This 1 mm diameter system is composed of a 0.1 NA relay lens

(1.75 pitch) and a 0.5 NA objective lens (<0.25 pitch), resulting in a total probe length of 8 cm. The fluorescence signal from the sample is epi-collected through the GRIN lenses and the microscope objective, and is reflected by a dichroic beam splitter (FF705-Di01, Semrock Inc.). After passing through one short pass filter (FF01-720/SP, Semrock Inc.), a notch dichroic (NFD01-532, Semrock Inc.) separates the signal into the second harmonic generation (SHG) and the autofluorescence channel. Another 520 nm bandpass filter (FF01-520/15, Semrock Inc.) is used to further minimize autofluorescence collection in the SHG channel. The housing of the GRIN lens endoscope is constructed from custom machined aluminum components using a milling machine with a fabrication tolerance of 0.001". Optical characterizations were conducted by moving the sample mounted on a 3D stage (MP-285, Sutter Instruments), allowing axial scanning of the sample while maintaining the GRIN lens endoscope system in a fixed position.

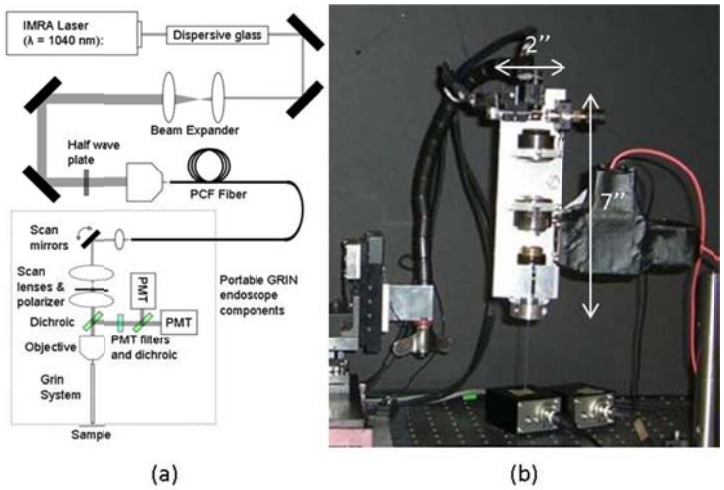

Figure 3.1. Portable GRIN lens endoscope. (a) Optical setup and (b) Photograph of the GRIN lens based endoscope system. Total system length of the portable device is 10.6" (including GRIN lens system).

To compensate for the fiber's anomalous dispersion, the pulses were pre-chirped by using a long piece of SF11 glass (Schott). Second order interferometric autocorrelations were performed to optimize the dispersion compensation by measuring the pulse-width at the sample for different lengths of SF11 glass before the fiber. We found that 65 cm of SF11 glass produced the shortest pulse with an intensity autocorrelation full-width at half-maximum (FWHM) of 509 fs. The resulting autocorrelation traces are shown in Figure 3.2.

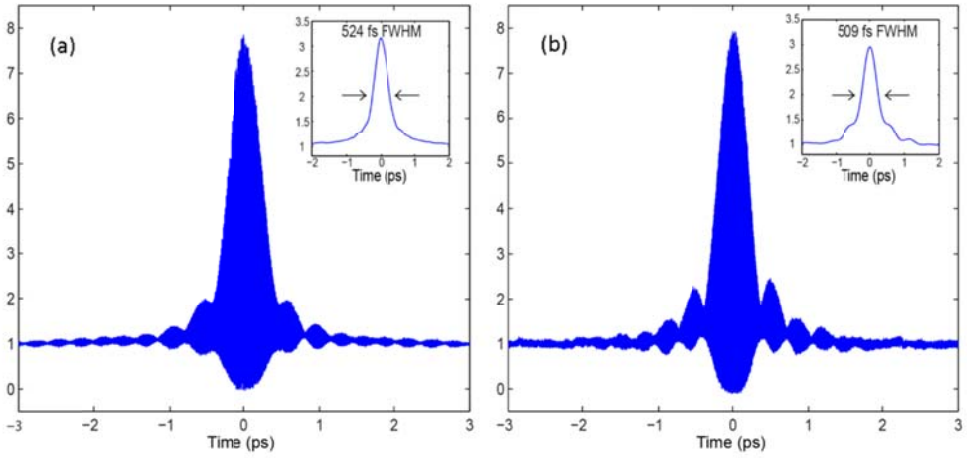

Figure 3.2. Second order interferometric autocorrelation traces of the pulse. (a) Directly from the source, inset: the corresponding intensity autocorrelation with a pulse width of 524 fs, (b) at the sample (i.e., after dispersion compensation using 65 cm of SF11 glass, the hollow core fiber, the optical components, and the GRIN lens), inset: the corresponding intensity autocorrelation with a pulse width of 509 fs.

We imaged fluorescent beads (0.1 µm diameter, absorption peak 350 nm , emission peak 440 nm, Invitrogen) embedded in agarose gel and with water immersion to characterize the lateral and axial 3P resolution. The FWHM for the lateral and axial resolution is 1.0 µm and 9.5 µm, respectively (Figure 3.3). To confirm 3P excitation, fluorescence signal was measured at 5 different excitation powers while the laser beam was fixed on a bead. Figure

3.3c shows that the fluorescence signal generated closely follows a cubic dependence on the excitation power. To demonstrate the capability of our device for imaging intrinsic fluorescence, we imaged unstained mouse lung tissue *ex vivo*. A 3 month old female, wild type mouse (Jackson Labs) was euthanized and a lung lobe was removed, embedded in agarose gel and plated on a standard glass microscope slide. The tissue was imaged within 1 hour of euthanasia using 5.9 mW at the sample and at a frame rate of 2 frames/s (512 by 512 pixels). Representative images are shown in Figure 3.4(a)-(c). We can identify the surface of the lung with strong SHG signal coming presumably from the pleura (Figure 3.4(a)). Below that, we can identify individual circular alveoli Figs.3. 4(b)-3.4(c), showing that the images could potentially provide diagnostic information. To confirm 3P excitation, fluorescence photons of the autofluorescence channel were measured at 5 different excitation powers at the sample by photon counting while scanning the laser beam at a fixed area in the tissue. Figure 3.4(d) shows that the fluorescence signal generated from the unstained tissue closely follows a cubic dependence on the excitation power, confirming that the image contrast is indeed generated by 3P excitation of intrinsic fluorescence.

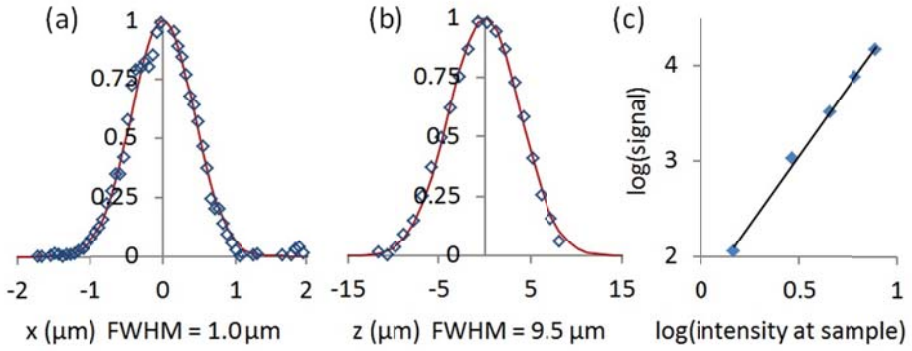

Figure 3.3. Three-photon lateral and axial resolution of the GRIN lens endoscope system. (a) Lateral and (b) axial intensity line profile across a subresolution fluorescent bead (blue diamonds). The Gaussian fits are indicated by the red lines. (c) Log-log plot of fluorescence signal as a function of excitation power at the sample. The slope is 2.9, indicating that the signal is generated by 3P excitation. Data in (c) was acquired using an ultrafast fiber laser at 1030 nm (Satsuma, Amplitude Systems, 5.7 MHz repetition rate).

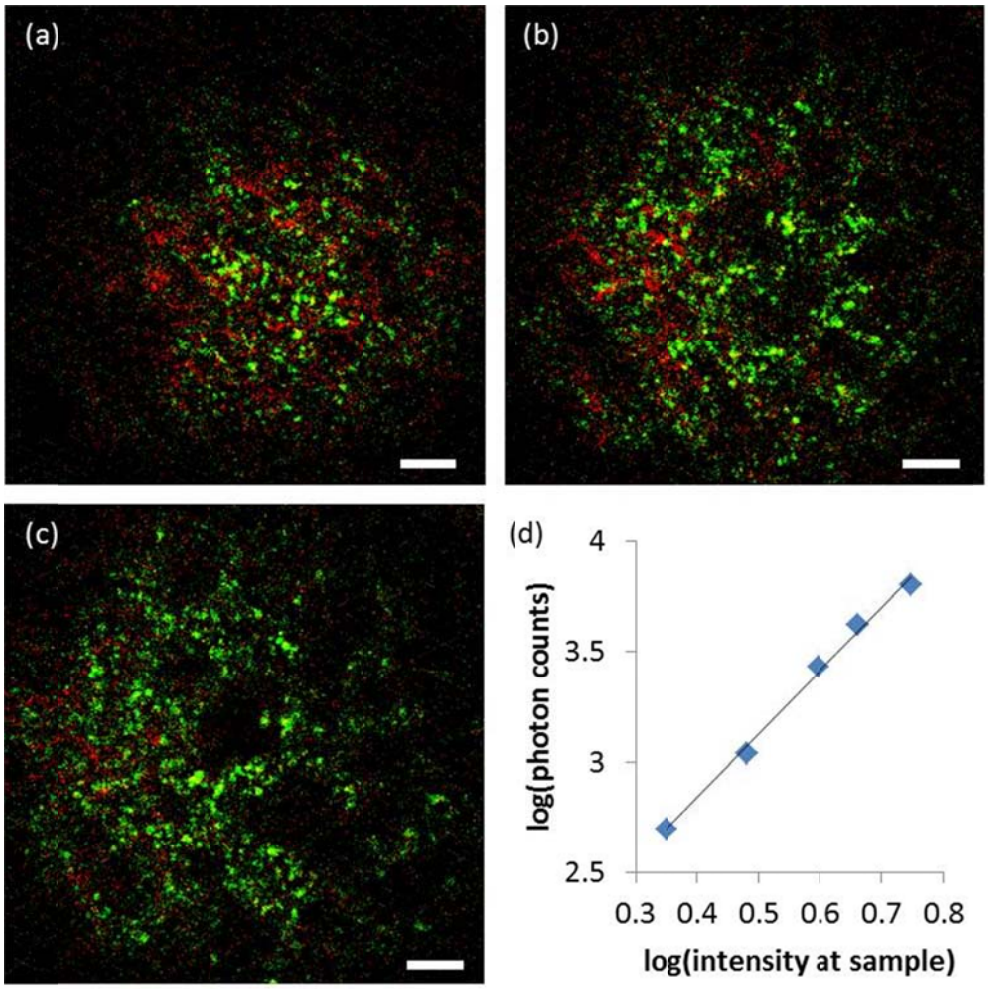

Figure 3.4. Unaveraged image of *ex vivo* unstained mouse lung acquired at 2 frames/s. Green: 3P autofluorescence. Red: SHG. Scale bar is 20 μm. Images taken at (a) 20 μm, (b) 30 μm, and (c) 40 μm below the tissue surface. (d) Log-log plot of autofluorescence signal as a function of excitation power at the sample. The slope is 2.9, indicating that the signal is generated by 3P excitation.

3.3. Discussion

Our results demonstrated the feasibility of 3P imaging of intrinsic fluorescence in a GRIN lens endoscope. As compared to our previous 2P imaging results at 800 nm using the same device [11], the resolution of 3P imaging at 1040 nm degrades slightly, 1.0 μm lateral and 9.5 μm axial for 3P imaging vs. 0.85 μm lateral and 7.4 μm

axial for 2P imaging. Since the GRIN lens system was originally designed for 800 nm excitation, the imaging performance at 1040 nm may be somewhat degraded. Nonetheless, our results showed that the spatial resolution is sufficient to provide diagnostic information.

There are several advantages for 3P endoscopy as compared to 2P endoscopy. The longer excitation wavelength and 3P excitation significantly improve the capability of tissue penetration [22], which is desirable for tissue diagnostics. 3P excitation allows the use of compact, convenient fiber femtosecond laser as the excitation source, which significantly reduces the cost and improves the clinical compatibility. Furthermore, the fiber laser at 1040 nm can excite intrinsic molecules (e.g., NADH, FAD) significantly closer to their 3P excitation peaks than 2P excitation at 800 nm [20]. While the pulse energy has increased in our demonstration as compared to our 2P endoscope, we found that the required average power for image generation is less than 6 mW, bringing multiphoton endoscopy to average power levels comparable to other optical diagnostic techniques such as confocal endoscopy and optical coherence tomography [23]. While the exact impact of pulse energy, duration, wavelength and average power on tissue damage needs to be investigated further, previous studies showed a lower phototoxicity at longer wavelengths [14,15,24]. We note that third harmonic generation (THG), which is much more ubiquitous than SHG, could potentially be added as another imaging contrast. Although THG imaging is not possible in our experiments because the transmission of the GRIN lens we used drops significantly below 370 nm, there is no fundamental limitation in making new lenses with high transmission at ~ 350 nm.

The main disadvantage of 3P endoscopy would be an increase in chromatic aberrations in the endoscope optics due to the larger difference between the excitation and signal wavelengths. The impact of this, however, can be reduced by carefully designing the optics for specific applications. Fiber delivery of the energetic femtosecond pulses for 3P excitation is another concern. The use of hollow core fibers, as shown in this paper, overcomes this difficulty. While hollow core fibers cannot effectively collect the fluorescence signal back through the excitation path, efficient signal collection through non-reciprocal optical path (e.g., using large core multimode fibers) has been demonstrated in the past [25,26]. Thus, 3P excitation can be implemented in a flexible endoscope with a small rigid tip.

It should be noted that although we used a fiber laser that is capable of producing average power up to 1 W (i.e., 1 μJ pulses), less than 6 mW (i.e., 6 nJ pulses) was used at the sample in our experiments. Compact, fiber based femtosecond oscillators producing >40 nJ pulse energy are commercially available. These sources are adequate for 3P excitation of intrinsic fluorophores assuming a reasonable system throughput of ~ 25%. Furthermore, our frame rate (2 frames per second) was limited by the low repetition rate of the laser (1MHz). Oscillators providing higher repetition rates (e.g., 3 MHz) and shorter pulses (e.g., 150 fs) can significantly increase the imaging acquisition rate without increasing the average excitation power, which will be valuable for overcoming motion artifacts for *in vivo* applications. Alternatively, the pixel clock of the image acquisition system could be synchronized to the laser pulses to maximize the frame rate [27], For example, 3 MHz repetition rate can provide a maximum frame rate of ~ 12 frames/s at 512 pixels by 512 pixels per frame, which is

adequate to overcome motion artifacts in in vivo imaging. Such a frame rate was shown to be adequate for *in vivo* imaging of Fluorescein stained human bladders using a confocal laser endoscope [28].

3.4. Conclusion

We have demonstrated the feasibility of 3P intrinsic fluorescence endoscopy using a GRIN lens endoscope and a fiber-based excitation source at 1040 nm. The compact and portable device can acquire 3P intrinsic fluorescence and SHG images at a rate of 2 frames/s with a field-of-view of ~200 μm diameter with subcellular resolution. The presented *ex vivo* results of unstained mouse lung tissue show great promise for using 3P GRIN lens endoscopy for optical biopsy. The combination of longer wavelength and 3P excitation, together with the convenient fiber-based excitation source, may make 3P endoscopy a valuable alternative to the conventional 2P approach.

Acknowledgements

This research was made possible by National Institutes of Health/National Cancer Institute Grant Number R01-CA133148 and National Institutes of Health/National Institute of Biomedical Imaging and Bioengineering Grant Numbers R01EB014873 and R01-EB006736. We thank members of the Xu and Schaffer-Nishimura research groups for discussions and technical suggestions.

References

1. W. Denk, J. H. Strickler, and W. W. Webb, “Two-photon laser scanning fluorescence microscopy,” Science **248**(4951), 73–76 (1990).
2. L. Fu, A. Jain, C. Cranfield, H. Xie, and M. Gu, “Three-dimensional nonlinear optical endoscopy,” J. Biomed. Opt. **12**(4), 040501 (2007).
3. M. T. Myaing, D. J. MacDonald, and X. Li, “Fiber-optic scanning two-photon fluorescence endoscope,” Opt. Lett. **31**(8), 1076–1078 (2006).
4. D. R. Rivera, C. M. Brown, D. G. Ouzounov, I. Pavlova, D. Kobat, W. W. Webb, and C. Xu, “Compact and flexible raster scanning multiphoton endoscope capable of imaging unstained tissue,” Proc. Natl. Acad. Sci. U.S.A. **108**(43), 17598–17603 (2011).
5. S. Tang, W. Jung, D. McCormick, T. Xie, J. Su, Y.-C. Ahn, B. J. Tromberg, and Z. Chen, “Design and implementation of fiber-based multiphoton endoscopy with microelectromechanical systems scanning,” J. Biomed. Opt. **14**(3), 034005 (2009).
6. Y. Wu, Y. Leng, J. Xi, and X. Li, “Scanning all-fiber-optic endomicroscopy system for 3D nonlinear optical imaging of biological tissues,” Opt. Express **17**(10), 7907–7915 (2009).
7. E. J. Seibel and Q. Y. J. Smithwick, “Unique features of optical scanning, single fiber endoscopy,” Lasers Surg. Med. **30**(3), 177–183 (2002).
8. D. R. Rivera, C. M. Brown, D. G. Ouzounov, W. W. Webb, and C. Xu, “Use of a lensed fiber for a large-field-of- view, high-resolution, fiber-scanning microendoscope,” Opt. Lett. **37**(5), 881–883 (2012).

9. D. R. Rivera, C. M. Brown, D. G. Ouzounov, W. W. Webb, and C. Xu, "Multifocal multiphoton endoscope," Opt. Lett. **37**(8), 1349–1351 (2012).

10. C. M. Brown, D. R. Rivera, I. Pavlova, D. G. Ouzounov, W. O. Williams, S. Mohanan, W. W. Webb, and C. Xu, "*In vivo* imaging of unstained tissues using a compact and flexible multiphoton microendoscope," J. Biomed. Opt. **17**(4), 040505 (2012).

11. D. M. Huland, C. M. Brown, S. S. Howard, D. G. Ouzounov, I. Pavlova, K. Wang, D. R. Rivera, W. W. Webb, and C. Xu, "*In vivo* imaging of unstained tissues using long gradient index lens multiphoton endoscopic systems," Biomed. Opt. Express **3**(5), 1077–1085 (2012).

12. D. Kobat, M. E. Durst, N. Nishimura, A. W. Wong, C. B. Schaffer, and C. Xu, "Deep tissue multiphoton microscopy using longer wavelength excitation," Opt. Express **17**(16), 13354–13364 (2009).

13. D. Kobat, N. G. Horton, and C. Xu, "*In vivo* two-photon microscopy to 1.6-mm depth in mouse cortex," J. Biomed. Opt. **16**(10), 106014 (2011).

14. I.-H. Chen, S.-W. Chu, C.-K. Sun, P.-C. Cheng, and B.-L. Lin, "Wavelength dependent damage in biological multi-photon confocal microscopy: A micro-spectroscopic comparison between femtosecond Ti:sapphire and Cr:forsterite laser," Opt. Quantum Electron. **34**(12), 1251–1266 (2002).

15. Y. Fu, H. Wang, R. Shi, and J.-X. Cheng, "Characterization of photodamage in coherent anti-Stokes Raman scattering microscopy," Opt. Express **14**(9), 3942–3951 (2006).

16. G. Liu, K. Kieu, F. W. Wise, and Z. Chen, "Multiphoton microscopy system with a compact fiber-based femtosecond-pulse laser and handheld probe," J. Biophotonics **4**(1-2), 34–39 (2011).

17. C. Xu, W. R. Zipfel, J. B. Shear, R. M. Williams, and W. W. Webb, "Multiphoton fluorescence excitation: new spectral windows for biological nonlinear microscopy," Proc. Natl. Acad. Sci. U.S.A. **93**(20), 10763–10768 (1996).

18. S. W. Hell, K. Bahlmann, M. Schrader, A. Soini, H. M. Malak, I. Gryczynski, and J. R. Lakowicz, "Three-photon excitation in fluorescence microscopy," J. Biomed. Opt. **1**(1), 71–74 (1996).

19. D. L. Wokosin, V. E. Centonze, S. Crittenden, and J. White, "Three-photon excitation fluorescence imaging of biological specimens using an all-solid-state laser," Bioimaging **4**(3), 208–214 (1996).

20. W. R. Zipfel, R. M. Williams, R. Christie, A. Y. Nikitin, B. T. Hyman, and W. W. Webb, "Live tissue intrinsic emission microscopy using multiphoton-excited native fluorescence and second harmonic generation," Proc. Natl. Acad. Sci. U.S.A. **100**(12), 7075–7080 (2003).

21. S. Maiti, J. B. Shear, R. M. Williams, W. R. Zipfel, and W. W. Webb, "Measuring serotonin distribution in live cells with three-photon excitation," Science **275**(5299), 530–532 (1997).

22. N. G. Horton, K. Wang, D. Kobat, C. G. Clark, F. W. Wise, C. B. Schaffer, and C. Xu, "*In vivo* three-photon microscopy of subcortical structures within an intact mouse brain," Nat. Photonics **7**(3), 205–209 (2013).

23. J. G. Fujimoto, C. Pitris, S. A. Boppart, and M. E. Brezinski, "Optical coherence tomography: an emerging technology for biomedical imaging and optical biopsy," Neoplasia **2**(1-2), 9–25 (2000).

24. J. M. Squirrell, D. L. Wokosin, J. G. White, and B. D. Bavister, "Long-term two-photon fluorescence imaging of mammalian embryos without compromising viability," Nat. Biotechnol. **17**(8), 763–767 (1999).

25. D. G. Ouzounov, D. R. Rivera, C. M. Brown, W. W. Webb, and C. Xu, "Dual modality microendoscope with optical zoom capability," in *CLEO 2012,* San Jose, CA (Optical Society of America, 2012), postdeadline paper ATh5A.2.

26. C. J. Engelbrecht, R. S. Johnston, E. J. Seibel, and F. Helmchen, "Ultra-compact fiber-optic two-photon microscope for functional fluorescence imaging *in vivo*," Opt. Express **16**(8), 5556–5564 (2008).

27. P. Theer, M. T. Hasan, and W. Denk, "Two-photon imaging to a depth of 1000 μm in living brains by use of a Ti:Al2O3 regenerative amplifier," Opt. Lett. **28**(12), 1022–1024 (2003).

28. G. A. Sonn, S. N. Jones, T. V. Tarin, C. B. Du, K. E. Mach, K. C. Jensen, and J. C. Liao, "Optical biopsy of human bladder neoplasia with *in vivo* confocal laser endomicroscopy," J. Urol. **182**(4), 1299–1305 (2009).

CHAPTER 4

MULTIPHOTON GRIN ENDOSCOPY FOR EVALUATION OF PROSTATIC TISSUE: TOWARDS REAL TIME HISTOLOGY IN UNSTAINED TISSUE[3]

Abstract

Multiphoton microscopy can instantly visualize cellular details in unstained tissues. Multiphoton probes with clinical potential have been developed. This study evaluates the suitability of a multiphoton GRIN endoscopy as a diagnostic tool for prostatic tissue. A portable and compact multiphoton endoscope based on a 1 mm diameter, 8 cm length GRIN lens system probe was used. Fresh *ex vivo* samples were obtained from 14 radical prostatectomy patients and benign and malignant areas were imaged and correlated with subsequent H&E sections. Multiphoton GRIN endoscopy images of unfixed and unprocessed prostate tissue at a subcellular resolution are presented. We note several differences and identifying features of benign versus low grade versus high grade tumors and are able to identify periprostatic tissues such as adipocytes, peri-prostatic nerves and blood vessels. Multiphoton GRIN endoscopy can be used to identify both benign and malignant lesion in *ex vivo* human prostate tissue and may be a valuable diagnostic tool for real-time visualization of suspicious areas of the prostate.

[3] The contents of this chapter have been reproduced from "Multiphoton GRIN Endoscopy for Evaluation of Prostatic Tissue: Towards Real Time Histology in Unstained Tissue", David M. Huland, Manu Jain, Dimitre G. Ouzounov, Brian D. Robinson, Diana S. Harya, Maria M. Shevchuk, Paras Singhal, Chris Xu, Ashutosh K. Tewari (in submission).

4.1 Introduction

Prostate cancer remains the most commonly diagnosed cancer in U.S men with approximately 240,000 new diagnosis in 2012 [1]. While approximately 28,000 men died of prostate cancer in 2012, the majority had indolent cancer that may be less likely to progress or cause death. Identifying these patients is difficult with current diagnostic techniques. Gleason score, which is obtained on biopsy, is by far the best predictor of cancer progression [2]. However, as only a fraction of the prostate gland is sampled and mostly in a blinded manner, prostate biopsies are only successful in detecting tumors in 60-70% of cases [3]. In prostates removed by radical prostatectomy (RP) an upstaging (>T2) is seen in 20.6% cases and an upgrading (Gleason score >6) in 44.9% cases was found on final histopathology [4]. As a consequence of such inaccuracies in staging and grading Prostate Cancer (Pca), non-indolent cancer candidates are often put under active surveillance (AS) leading to cancer progression. Furthermore, many suitable candidates are not enrolled in AS and receive unnecessary over-treatment with concomitant side effects.

RP is frequently selected treatment option for men with localized prostate cancer. However, a significant challenge faced by surgeons during RP is the complete removal of the cancerous tissue, while preserving the nerves surrounding the prostate that are responsible for continence and erectile function. These nerves, as well as the malignant glands, are too small to be visualized by eye. Although, RP with the da Vinci robotic surgical system allows for a significant advantage in surgical precision due to 10-12x magnification of the surgical field, it lacks the cellular resolution to

differentiate cancerous cells from surrounding nerve tissue. Thus the surgeons rely on intraoperative frozen section (IFS) analysis to provide some benefit in reducing positive surgical margins (PSMs) [5]. However, frozen sections require time and, only provide an assessment of a fraction of the area of interest. Further, as IFS requires the removal of tissue, there is always a risk of damaging the area one is trying to preserve, especially the peri-prostatic nerves. As a result, RP's have PSMs [6–9] in 10 - 40% of cases and a 25 - 70% rate of postoperative impotence [10–14]. In essence, inaccurate disease quantification, staging and unavailability of intraoperative pathological guidance often results in mismatched treatment recommendations, over treatment, residual cancer (positive surgical margins) during surgery and need for expensive radiation treatment to salvage these cancers. Thus, for both the diagnosis and the treatment of prostate cancer a faster and more accurate way of characterizing the tissue at a cellular level could significantly improve decision making during treatment and patient outcomes.

Multiphoton microscopy (MPM) provides the ability to image fresh, unprocessed (unstained and unfixed) tissues at subcellular resolution *in vivo* [15–17]. It has been demonstrated to provide tissue architecture comparable to gold standard H&E and has been shown as a valuable tool in the diagnosis of benign and malignant lesions in multiple organs including the lung [18,19], bladder [20], and ovaries [21]. Its ability to image unprocessed and unstained human prostate tissue *ex vivo* has further shown that MPM can identify relevant prostatic and periprostatic tissues and pathological changes [22,23]. Although these studies serve as a baseline to establish the signature of

the various tissue types and pathologies on MPM, the bench top MPM microscope, used in these studies cannot be used *in vivo* intraoperatively.

We have previously reported on a compact and portable GRIN based endoscope for clinical multiphoton applications[24,25]. The design of this device is centered around a rigid 8 cm length, 1 mm diameter GRIN endoscopic probe and can image a 200 μm diameter field-of-view at 4 frames per second (512 * 512 pixels) at subcellular resolution. We have demonstrated the device through *in vivo* imaging of the kidney, colon and liver in anesthetized rats. In this study we test the diagnostic capabilities of our GRIN endoscope on *ex vivo* human prostate samples obtained from radical prostatectomy patients.

4.2 Portable & Compact GRIN Endoscope System

The compact and portable GRIN endoscope system is shown in Figure 4.1 and was previously described [24,25]. In brief, the near infra-red excitation pulses are delivered to the device via a ~2 m hollow core photonic band-gap fiber. After being collimated by a aspheric lens on the portable GRIN lens endoscope, the beam is scanned by a two-axis galvanometer scan mirror system, and two scan lenses and a 0.3 NA objective are used to scan the back of the GRIN lens endoscope system. This is composed of a 0.1 NA relay lens (1.75 pitch) and a 0.5 NA objective lens (<0.25 pitch). For the *ex vivo* human tissue demonstration at Weill Cornell Medical Center we used a turn-key, compact fiber laser system at 780 nm with a repetition rate of 50MHz (Carmel, Calmar Laser). Due to the shifted wavelength closer to the zero dispersion

wavelength of the fiber as compared to our previous demonstration at 800 nm [24], we were able to remove the piece of dispersive glass used for dispersion compensation before, yielding a pulse width of ~150 fs at the sample. The fluorescence signal from the sample is epi-collected through the GRIN system and the microscope objective, and is reflected by two dichroic beam splitters and collected into two different channels for autofluorescence (~405 -700 nm) and second harmonic generation (SHG) (<405 nm). The resulting system weighs less than 2 lbs and can image a 200 μm diameter field-of-view at 4 frames per second (512 * 512 pixels) at subcellular resolution. Resulting images were post processed to improve contrast and brightness levels and pseudo-colored with autofluorescence in green and SHG in red.

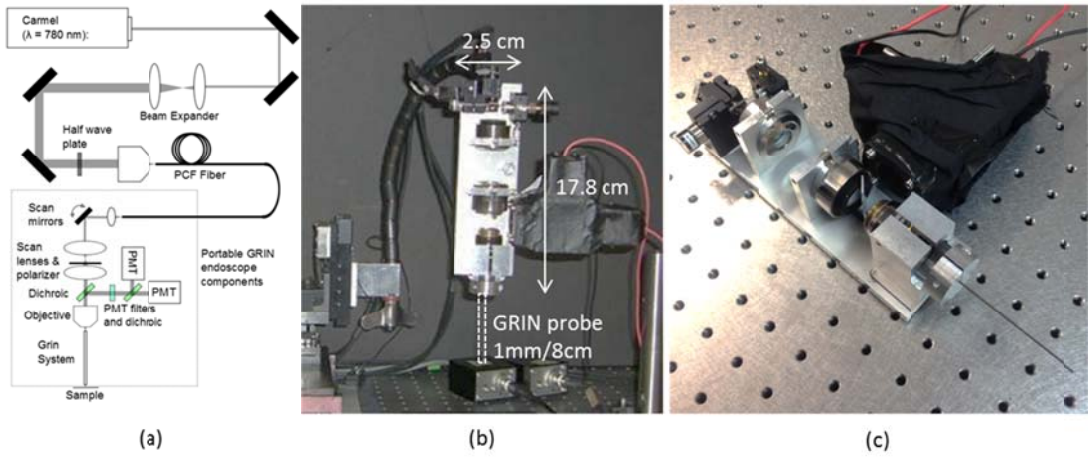

Figure 4.1 - Portable GRIN endoscope. (a) Optical drawing and (b) photograph of the GRIN based endoscope system as mounted for imaging and (c) close up of the portable GRIN endoscope.

4.3 Ex vivo human prostate imaging

The present study included 14 robotic radical prostatectomies from patients who agreed to participate in an Institutional Review Board approved study. Patients age ranged from 41-75 years. Prostates removed by RP were first taken to the Department of Surgical Pathology for gross examination. One specimen was imaged intact immediately after RP to identify peri-prostatic tissue. For the rest of the 13 specimens, surfaces were inked as per institutional protocol and then specimens were sliced in roughly 0.5-cm thick sections. One section per specimen with visible tumor or most likely to have tumor was chosen by a uropathologist. The sections were brought to the multiphoton endoscopy facility in normal saline and imaged at room temperature with the GRIN endoscope. All the sections were imaged under the guidance of research pathologist experienced with MPM imaging. Images were acquired from areas labeled as benign and malignant on gross inspection of the section. Unless otherwise noted, all samples were imaged within ~3hrs of excision from the patient, and at 50 mW at the sample and at 4 frames per second. During imaging the sample was fixed in agar gel to reduce motion artifacts. 0.9% phosphate buffered saline (PBS) was used for GRIN objective immersion and to prevent the tissue from drying out. Throughout the imaging sessions, the portable GRIN endoscope was mounted on 3D stage for fine movement control. After imaging, the specimen was returned to the Department of Surgical Pathology in 10% buffered formalin and processed for routine histopathology (formalin fixation, embedding, sectioning and staining). All H&E images shown in the figures were taken under oil immersion objective (100X) with total magnification of 1000X to match the field-of-view (FOV) of ~150 μm x 150 μm on MPM. H&E comparison images were taken

from the same sample and of a similar area of the site where the original multiphoton endoscopy image was taken.

4.4 Results:

MPM imaging of Prostate gland: The prostate gland is composed of mainly two components: acini and fibromuscular stroma. In the multiphoton endoscopy images of the benign prostatic tissue (Figure 4.2), we could identify benign glands based on their architecture i.e. large gland with infolded epithelium and ill-defined luminal border. In addition, strong punctate autofluorescence in the cytoplasm was uniquely seen in the benign glands. This signal most likely originates from lipofuscin found abundantly in cytoplasm of the benign glands. Some benign glands were seen lined by flattened epithelium with secretions/concretions in their lumen. Similarly, the fibromusclar stroma had strong SHG signal generated by collagen along with autofluorescent muscle fibers and some elastin fibers. By comparsion, the images taken from areas with adenocarcinoma (Figure 4.3) showed clusters of small acini with sharp luminal borders and some aggregated small secretions in the lumen. These areas were confirmed to have low grade tumor (Gleason 3+3=6) on H&E. In the areas confirmed as high grade (Gleason 7+) adenocarcinoma on H&E, MPM images showed loss of normal architecture and it was challenging to identify individual acini. Furthermore, SHG signal was significantly reduced in areas of high grade tumor as compared to areas of low grade tumor.

MPM imaging of peri-prostatic tissue: In addition to imaging sections from the prostate glands, in one case we imaged the surface of intact RP specimen to simulate intraoperative margin imaging. Here we could identify relevant periprostatic tissues, such as adipocytes, peri-prostatic nerves and blood vessels (Figure 4.4). Adipocytes were recognized based on their globular shape and homogenous cytoplasm. Nerve was clearly identified by its wavy nerve fibers and was distinguishable from blood vessel due to lack of lumen.

Being able to obtain histology quality images at lower excitation powers could be beneficial to reduce concerns about the safety of multiphoton endoscopy. In Figure 4.5 we reduce the power to 32 mW while keeping the frame rate constant at 4 frames/s (Figure 4.5B). While the signal-to-noise ratio in the image is decreased, most of the architecture is still visible as compared to the original image at 50 mW. Similarly, if motion artifacts could be overcome to a point where longer integration times are not a problem, Figure 4.5E shows that we can obtain images of very comparable quality at 6mW excitation power when averaging 16 frames obtained at 1 frame /s (i.e. 16 seconds total acquisition time).

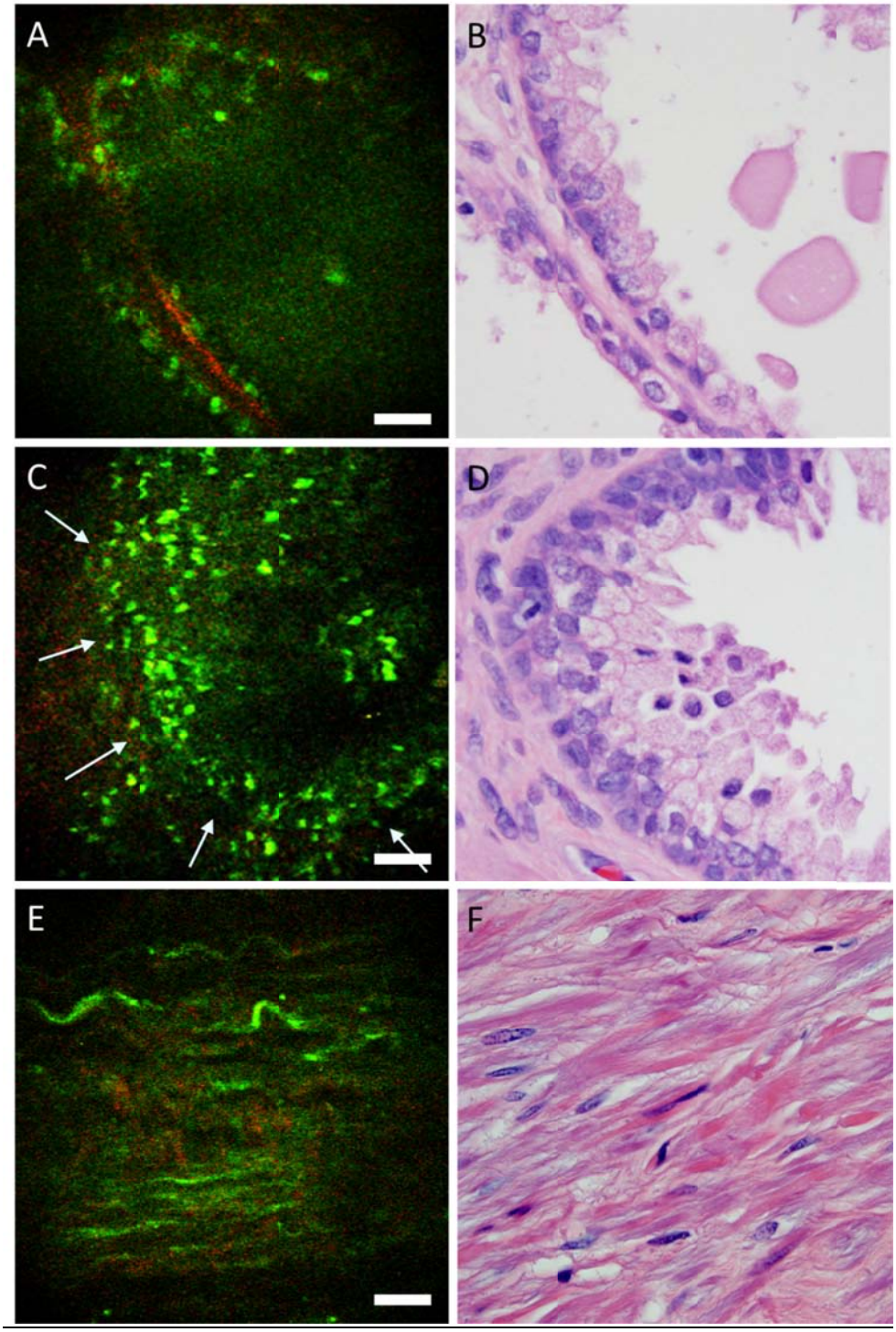

Figure 4.2 – *Ex vivo* imaging of benign prostatic tissue. (A,C) Multiphoton endoscopy images of benign prostatic glands (arrows) with (A) flat epithelium along with secretion/concretions and (C) infolded epithelium and ruffled luminal border in the lumen. (E) Multiphoton endoscopy image of stroma. Scale bars are 20 µm (B,D, F) Corresponding H&E stained sections. H&E: Total magnification = 1000X

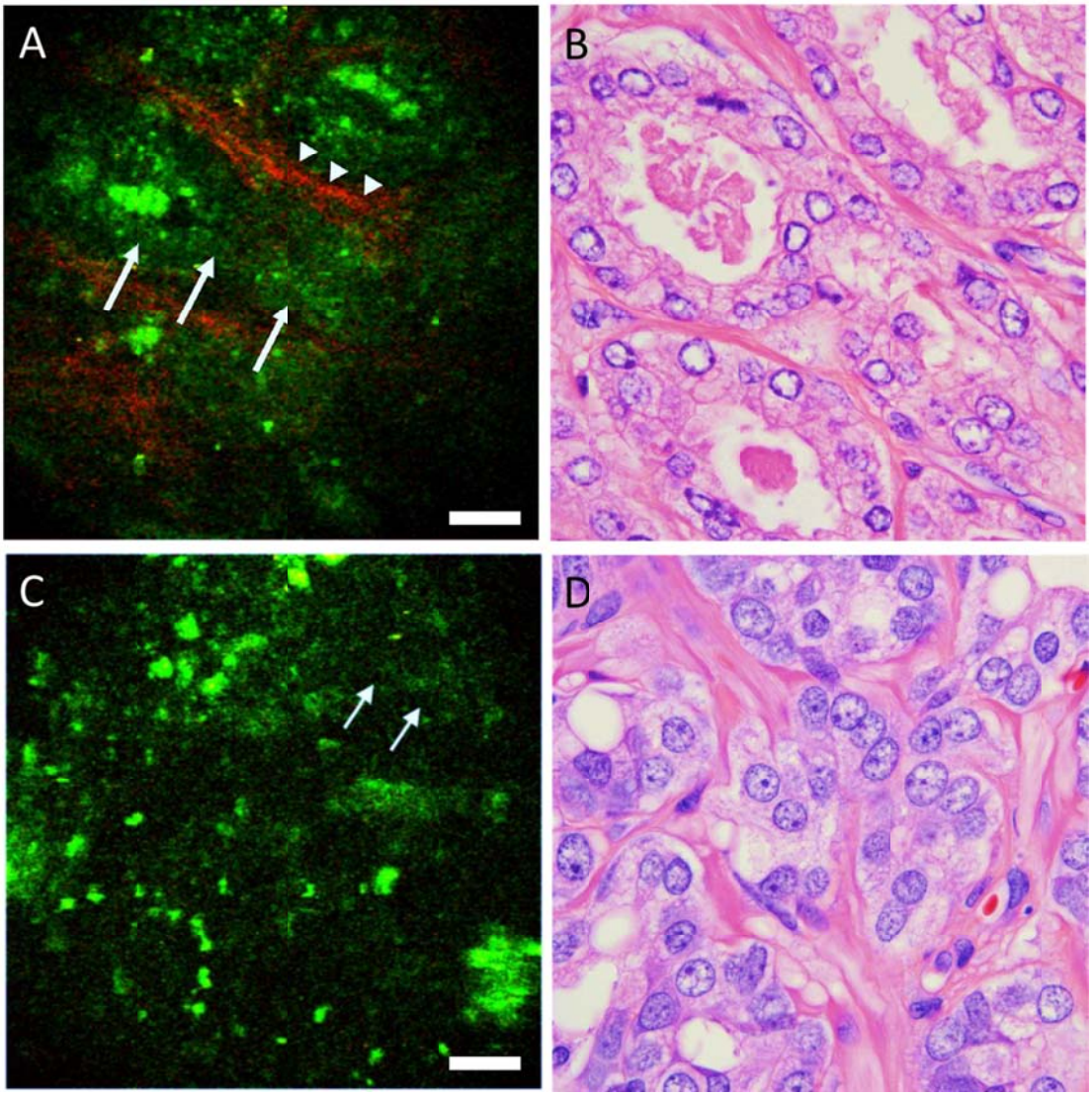

Figure 4.3 – *Ex vivo* imaging of prostate tumor. (A,C) Multiphoton endoscopy images of adenocarcinoma prostate showing (A) an example of a low grade tumor area with clusters of tiny glands (arrows) with sharp luminal borders (arrowheads) and (C) example of a high grade tumor areas of irregularly shaped or poorly formed glands and nests of cells (arrows). Scale bars are 20 µm. And (B,D) corresponding H&E images. H&E: Total magnification = 1000X.

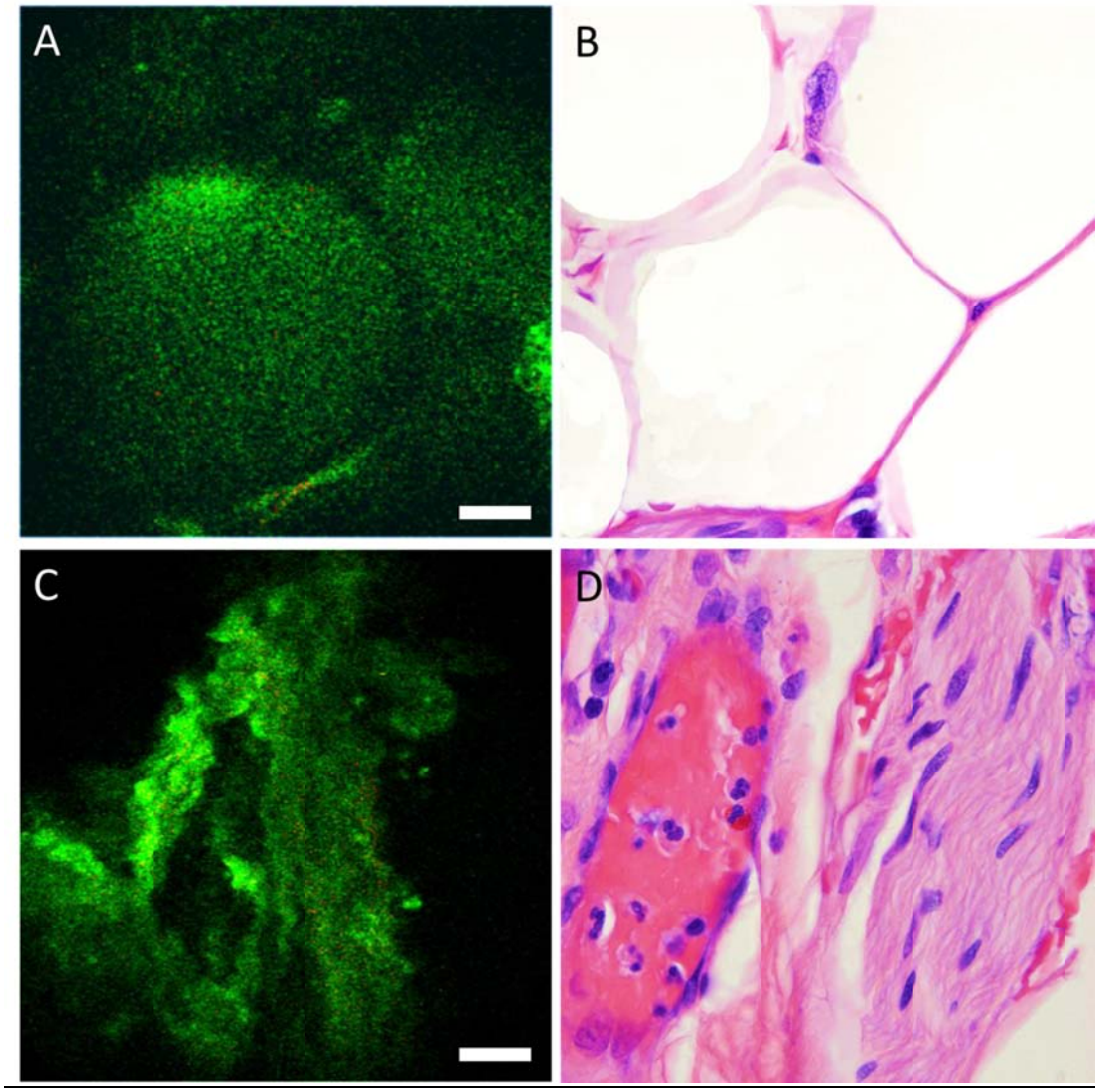

Figure 4.4 – *Ex vivo* imaging of peri-prostatic tissue. (A) Multiphoton endoscopy image of adipocytes, and (C) a neurovascular bundle. Scale bars are 20 μm. And (B,D) corresponding H&E images. H&E: Total magnification = 1000X

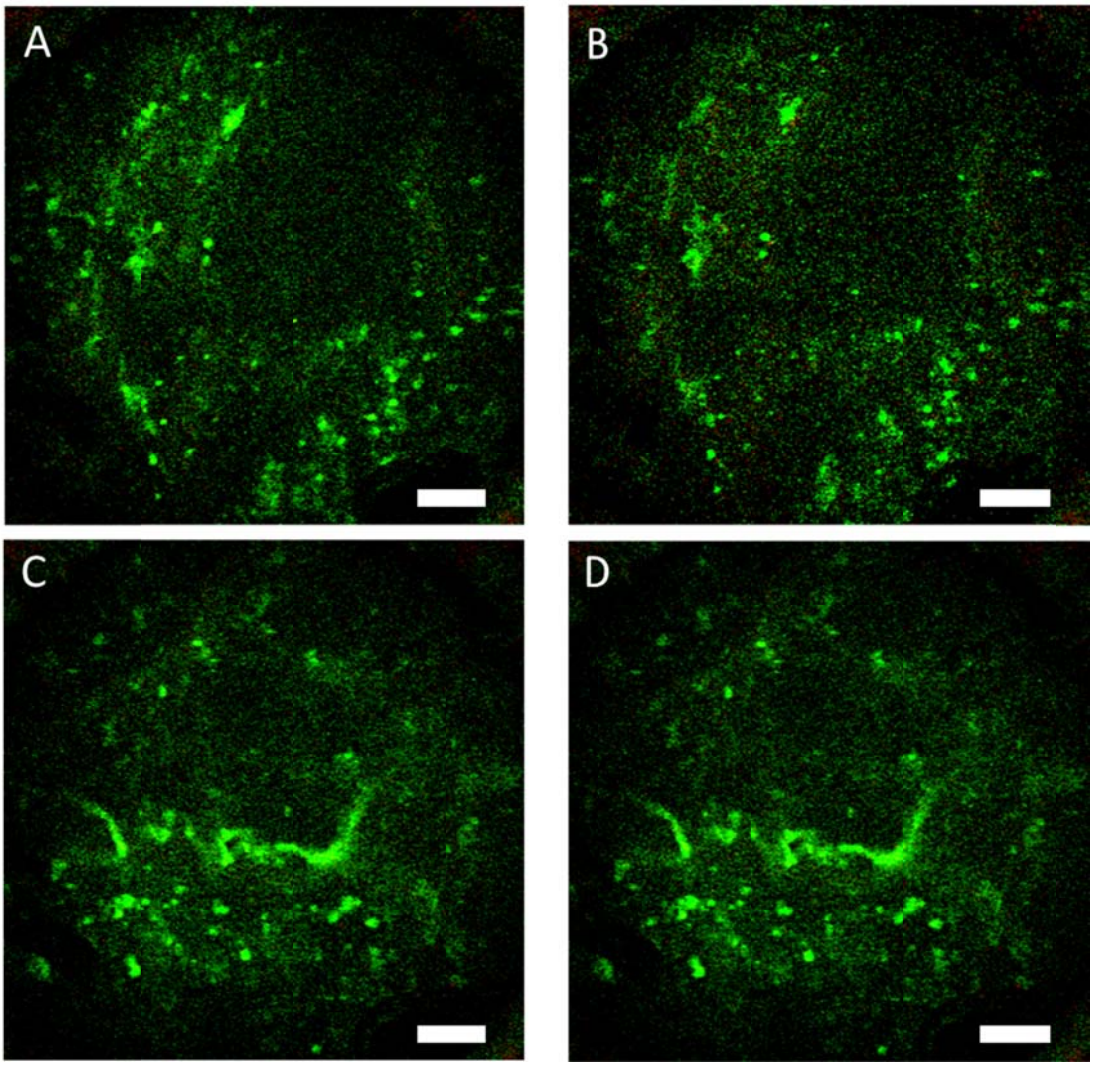

Figure 4.5 – *Ex vivo* human prostate imaging and averaging. (A,C) Multiphoton endoscopy images of prostate showing (A) a ~150 µm x 150 µm field-of-view taken at 4 frames / s and 50mW excitation power at the sample. (B) Frame rate kept constant at 4 frames/ s and excitation power reduced to 32mW. (D) Excitation power reduced to 6mW and 16 frames averaged at 1 frame/s (i.e. 16 seconds / frame). Scale bars are 20 µm.

4.5 Discussion

We have demonstrated that multiphoton GRIN endoscopy can image fresh, unfixed and unprocessed prostate tissue at a subcellular resolution. We can not only identify but also differentiate areas with benign glands from areas with

adenocarcinoma in *ex vivo* prostate sections. In addition, we identified important peri-prostatic tissues such as nerves, adipocytes and blood vessels. This study demonstrates the feasibility and lays the foundation for future *in vivo* imaging in prostate cancer patients to improve their diagnosis and management.

Images obtained from the *in vivo* rat experiment demonstrates multiphoton GRIN endoscopy as a potential tool for *in vivo* imaging in human subjects, intra-operatively. As we have previously described [24] the main source of motion artifacts during *in vivo* rat experiments is movement from the diaphragm during respiration. While we were able to isolate this motion successfully during this demonstration, the exact effect of this on the quality of the images during surgery needs to be investigated. We would anticipate the respiratory motion to be less significant in human subjects due to significantly slower respiratory rate and a considerable distance of pelvis from the diaphragm. However, one could expect more contribution from cardiovascular motion in a human subject. The pneumoperitoneum created during robotic RP could help significantly in reducing the effect of both cardiac and pulmonary motion artifacts.

The ultimate goal of multiphoton endoscopy is to achieve a real time visualization of prostatic tissue in clinical setting. Based on the images obtained in this study and the fact that this device is potentially compatible in dimensions (8cm length x 1mm diameter) with a biopsy needle, we envision its integration in the prostate biopsy gun to carry out targeted biopsies. By achieving real time histology, we can improve the diagnostic accuracy of the Gleason grading by increasing the yield of

cancerous tissue (by sampling the suspicious area) for histopathological diagnosis during biopsy procedure. This can be a valuable tool for better selection of active surveillance patients and reduce the rate of under or overtreatment. This device could also be used intra-operatively during radical prostatectomy to identify periprostatic nerves and to assess surgical margins, thus potentially reducing complications associated with RP such as erectile dysfunction and urinary incontinence, resulting in improved functional outcomes and quality of life for the patients.

Before this endoscopic device can be integrated into routine clinical workflow, several potential challenges need to be addressed. The most significant one is probably proving that the excitation powers used are not harmful to the imaged tissue. We have shown that if motion artifacts could be reduced significantly, excitation powers as low as 6 mW would be sufficient for similar quality images. Additionally, several studies have suggested that the higher power levels used in this study are below the threshold for DNA and other tissue damage [16,26]. However, due to multiple factors potentially influencing these thresholds (including numerical aperture, wavelength, pulse width, aberrations in the optical system, and exposure time), the exact threshold needs to be characterized for the presented endoscope.

Further, the clinical environment may provide new challenges, such as cardiac motion and blood interfering with the imaging. The presented endoscope can image a 200 μm field-of-view at 4 frames/s. Motion artifacts could be overcome by increasing the frame rate further and strategies have been suggested to achieve this [27]. Challenges involving blood and other tissues interfering with the images could be

overcome by adding the ability to flush the surface of the endoscope with saline. The major limitation from diagnostic point of view is the very small field-of-view of 200 μm that limits the area under inspection and impedes architectural analysis. A larger field-of-view would be advantageous to scan a larger fraction of the prostate to give an idea of overall architecture under imaging. At the cost of resolution, one could increase the field-of-view by decreasing the objective NA used. Although in our study the field-of-view appeared sufficient to generally distinguish benign from malignant tissue and we were able to identify areas with low grade and high grade tumor, a larger sample size and further studies are needed to verify this claim.

In summary, we have shown that multiphoton GRIN endoscopy can be used to identify both benign and malignant lesion in *ex vivo* human prostate tissue. The GRIN endoscope is integrated into a compact and portable device that could potentially be used in a clinical setting for guided biopsies or intra-operative assessment of peri-prostatic nerves and prostatic margins. This may reduce complications associated with over/under treatment and improve functional outcomes and quality of life for prostate cancer patients.

Acknowledgements

We thank members of the Xu, and Tewari research groups for discussions and technical suggestions. We also thank Alexander Nikitin of the Department of Biomedical Sciences at the Cornell University College of Veterinary Medicine for discussions and technical suggestions. We also thank Jiny Li of the Department of

Urology at the Weill Cornell Medical College for laboratory work. Our project was supported by the National Institutes of Health (NIH)/National Cancer Institute grant R01-CA133148 and the NIH/National Institute of Biomedical Imaging and Bioengineering grant R01-EB006736.

REFERENCES

1. Siegel R, Naishadham D and Jemal A: Cancer statistics, 2012. CA. Cancer J. Clin. **62**: 10–29.
2. Cheng L, Koch MO, Juliar BE, et al: The combined percentage of Gleason patterns 4 and 5 is the best predictor of cancer progression after radical prostatectomy. J. Clin. Oncol. 2005; **23**: 2911–7.
3. Chun FK-H, Epstein JI, Ficarra V, et al: Optimizing performance and interpretation of prostate biopsy: a critical analysis of the literature. Eur. Urol. 2010; **58**: 851–64.
4. El Hajj A, Ploussard G, de la Taille A, et al: Analysis of outcomes after radical prostatectomy in patients eligible for active surveillance (PRIAS). BJU Int. 2013; **111**: 53–9.
5. Dillenburg W, Poulakis V, Witzsch U, et al: Laparoscopic radical prostatectomy: the value of intraoperative frozen sections. Eur. Urol. 2005; **48**: 614–621.
6. Smith RC, Partin a W, Epstein JI, et al: Extended followup of the influence of wide excision of the neurovascular bundle(s) on prognosis in men with clinically localized prostate cancer and extensive capsular perforation. J. Urol. 1996; **156**: 454–7; discussion 457–8.
7. Wieder J a and Soloway MS: Incidence, etiology, location, prevention and treatment of positive surgical margins after radical prostatectomy for prostate cancer. J. Urol. 1998; **160**: 299–315.

8. Watson R, Civantos F and Soloway M: Positive surgical margins with radical prostatectomy: detailed pathological analysis and prognosis. Urology 1996; **5**.

9. Sofer M, Hamilton-Nelson KL, Schlesselman JJ, et al: Risk of positive margins and biochemical recurrence in relation to nerve-sparing radical prostatectomy. J. Clin. Oncol. 2002; **20**: 1853–1858.

10. Bentas W, Wolfram M, Jones J, et al: Robotic Technology and the Translation of Open Radical Prostatectomy to Laparoscopy: The Early Frankfurt Experience with Robotic Radical Prostatectomy and One Year Follow-up. Eur. Urol. 2003; **44**: 175–181.

11. Ahlering TE, Skarecky D, Lee D, et al: Successful transfer of open surgical skills to a laparoscopic environment using a robotic interface: initial experience with laparoscopic radical prostatectomy. J. Urol. 2003; **170**: 1738–41.

12. Eden C, Cahill D and Vass J: Laparoscopic radical prostatectomy: the initial UK series. BJU … 2002: 876–882.

13. Rassweiler J and Marrero R: Transperitoneal laparoscopic radical prostatectomy: ascending technique. J. … 2004; **18**.

14. Saranchuk JW, Kattan MW, Elkin E, et al: Achieving optimal outcomes after radical prostatectomy. J. Clin. Oncol. 2005; **23**: 4146–51.

15. Denk W, Strickler J and Webb W: Two-photon laser scanning fluorescence microscopy. Science (80-.). 1990; **248**: 73–76.

16. Dela Cruz JM, McMullen JD, Williams RM, et al: Feasibility of using multiphoton excited tissue autofluorescence for in vivo human histopathology. Biomed. Opt. Express 2010; **1**: 1320–1330.

17. Zipfel WR, Williams RM, Christie R, et al: Live tissue intrinsic emission microscopy using multiphoton-excited native fluorescence and second harmonic generation. Proc. Natl. Acad. Sci. U. S. A. 2003; **100**: 7075–80.

18. Jain M, Narula N, Aggarwal A, et al: Multiphoton Microscopy: A Potential "Optical Biopsy" Tool for Real-Time Evaluation of Lung Tumors Without the Need for Exogenous Contrast Agents. Arch. Pathol. Lab. Med. 2013.

19. Pavlova I, Hume KR, Yazinski SA, et al: Multiphoton microscopy and microspectroscopy for diagnostics of inflammatory and neoplastic lung. J. Biomed. Opt. 2012; **17**: 036014.

20. Jain M, Robinson BD, Scherr DS, et al: Multiphoton microscopy in the evaluation of human bladder biopsies. Arch. Pathol. Lab. Med. 2012; **136**: 517–26.

21. Williams RM, Flesken-Nikitin A, Ellenson LH, et al: Strategies for high-resolution imaging of epithelial ovarian cancer by laparoscopic nonlinear microscopy. Transl. Oncol. 2010; **3**: 181–94.

22. Tewari AK, Shevchuk MM, Sterling J, et al: Multiphoton microscopy for structure identification in human prostate and periprostatic tissue: implications in prostate cancer surgery. BJU Int. 2011; **108**: 1421–9.

23. Yadav R, Mukherjee S, Hermen M, et al: Multiphoton microscopy of prostate and periprostatic neural tissue: a promising imaging technique for improving nerve-sparing prostatectomy. J. Endourol. 2009; **23**: 861–7.

24. Huland DM, Brown CM, Howard SS, et al: In vivo imaging of unstained tissues using long gradient index lens multiphoton endoscopic systems. Biomed. Opt. Express 2012; **3**: 1077–85.

25. Huland DM, Charan K, Ouzounov DG, et al: Three-photon excited fluorescence imaging of unstained tissue using a GRIN lens endoscope. Biomed. Opt. Express 2013; **4**: 652–8.

26. Ramasamy R, Sterling J, Fisher ES, et al: Identification of Spermatogenesis With Multiphoton Microscopy: An Evaluation in a Rodent Model. J. Urol. 2011; **186**: 2487–2492.

27. Rivera DR, Brown CM, Ouzounov DG, et al: Multifocal multiphoton endoscope. Opt. Lett. 2012; **37**: 1349–51. Available at: http://ol.osa.org/abstract.cfm?URI=ol-37-8-1349, accessed December 13, 2013.